JOURNAL OF SPACECRAFT AND ROCKETS
Vol. 45, No. 2, March–April 2008

Optimal Deployment/Retrieval of Tethered Satellites

Paul Williams*
Balwyn North, Victoria 3104, Australia

DOI: 10.2514/1.31804

The deployment and retrieval processes of a tethered satellite system are studied from the point of view of optimal control. In the past, the application of various optimality criteria, such as minimum tension or minimum libration angles, have been applied in the determination of open-loop deployment and retrieval trajectories. This paper demonstrates by way of numerical examples that these criteria are inappropriate for defining the reference trajectories. By applying various optimality criteria, such as minimum tension rate, minimum length acceleration, and so on, as well as minimax optimal control techniques, it is shown that the best control objectives should incorporate the minimization of system accelerations. Both inelastic and elastic tethers are considered, and it is proven that the deployment and retrieval reference trajectories are symmetrical under certain conditions. The importance of selecting an appropriate cost function is highlighted and the numerical results provide a good reference for mission planners.

Nomenclature

EA	=	tether longitudinal stiffness, N
$\mathcal{J}$	=	cost function for optimization
L_f	=	reference tether length, m
l	=	tether total length; length of rigid tether, m
l_0	=	unstrained tether length, m
m	=	total system mass, kg, $m_1 + m_2 + m_t$
m_t	=	deployed tether mass, kg, ρl_0
m^*	=	reduced system mass, kg, $(m_1 + m_t/2)(m_2 + m_t/2)/m - m_t/6$
$\bar{m}$	=	kg, $m_1(m_2 + m_t)/m$
m_1	=	mother satellite mass, kg, $m_1^0 - m_t$
m_2	=	subsatellite mass, kg
m_1^0	=	mother satellite mass before deployment of the tether, kg
R	=	orbit radius of system center of mass, m
T	=	tether tension, N
u	=	nondimensional tether tension control input, $T/\{m_1(m_2 + m_t)\omega^2 L_f/m\}$
x	=	position of tether end mass in the orbital frame along local vertical axis
y	=	position of tether end mass in the orbital frame along local horizontal axis
ε	=	tether longitudinal strain
θ	=	in-plane tether libration angle, deg
Λ	=	nondimensional tether length, l/L_f
Λ_0	=	nondimensional unstrained tether length, l_0/L_f
ρ	=	tether line density, kg/m
ω	=	orbital angular velocity, rad/s

Superscripts

$(\,)'$	=	nondimensional time derivative, $\mathrm{d}(\,)/\mathrm{d}(\omega t)$
$\dot{(\,)}$	=	time derivative, $\mathrm{d}(\,)/\mathrm{d}t$

Presented as Paper 4291 at the Joint Propulsion Conference, Tucson, AZ, 10–13 July 2005; received 26 April 2007; revision received 4 October 2007; accepted for publication 18 October 2007. Copyright © 2007 by Paul Williams. Published by the American Institute of Aeronautics and Astronautics, Inc., with permission. Copies of this paper may be made for personal or internal use, on condition that the copier pay the $10.00 per-copy fee to the Copyright Clearance Center, Inc., 222 Rosewood Drive, Danvers, MA 01923; include the code 0022-4650/08 $10.00 in correspondence with the CCC.

*Research Fellow, Unit 1, 4 Maylands Avenue; tethered.systems@gmail.com. Member AIAA.

I. Introduction

TETHERED satellite systems are extremely important for many future space applications [1]. Momentum transfer [2–4] and electrodynamic maneuvering [5–8] represent possible propellantless transportation applications of space tethers. A large number of studies on the dynamics and control of tethered satellites has been undertaken since tethered satellites were first proposed for studying the upper atmosphere (see Misra and Modi [9] and Williams [10] and the references contained therein). Two of the most fundamental maneuvers that must be performed by tethered satellite systems are deployment and retrieval. Retrieval is regarded to be much more difficult to control than deployment because it is naturally unstable [9]. Although deployment is an inherently stable operation provided certain deployment rates are not exceeded, careful control is still necessary to achieve a desired terminal configuration. Examples of terminal orientations of the tether are along the local vertical for circular orbits [9], periodic motion for elliptical orbits [11], or a large prescribed swing rate for tether-assisted reentry maneuvers [12].

Among the strategies that have been used to control deployment and retrieval are linear feedback [13], mission function (Lyapunov) control [14–16], and optimal control [17–19]. Optimal control theory is perhaps best suited for controlling deployment and retrieval because it allows accurate maneuvering of the system between initial and terminal states. The application of optimal control techniques to the deployment and retrieval operations of tethered satellites has been undertaken using different approaches by Fujii and Anazawa [17], Williams et al. [20], Lakso and Coverstone [21], and Steindl and Troger [19]. In all of these cases, the tether has been treated as an inextensible rigid rod, although numerical simulations for a flexible tether were carried out in Williams et al. [20].

Fujii and Anazawa [17] determined optimal trajectories for deployment and retrieval to minimize a performance index containing a linear combination of the squares of the nondimensional tension and in-plane libration angle using the conjugate-gradient method. Barkow et al. [22] determined optimal deployment trajectories to minimize a performance index containing a combination of the deployment time and the square of the in-plane libration angle using a multiple shooting method. Barkow et al. [22] constrained the tether length rate to be nonnegative (i.e., braking only deployment). Koakutsu et al. [23] considered optimal deployment control for a microsatellite using a sequential conjugate restoration algorithm to minimize the integral square of the tether length rate and also included a term to keep the tether tension large. The performance index was selected by physical considerations for the deployment tracking controller. Lakso and Coverstone [21] determined optimal deployment and retrieval trajectories using a Hermite–Simpson direct collocation approach to minimize the integral square of the nondimensional tether tension. Zimmerman et al. [24] determined

optimal deployment trajectories for a tether-assisted reentry mission to minimize the integral square of the nondimensional control tension using a multiple shooting method. Andres et al. [25] determined optimal trajectories for the initial phase of the tether-assisted deorbit maneuver considered by Zimmerman et al. [24] and also minimized the integral square of the nondimensional tension. Andres et al. [25] also applied a linear quadratic feedback controller to minimize deviations of the tether state from the reference trajectory over an infinite horizon. Nagata [26] considered the optimal control of a tether system with small end masses, taking into consideration both the tether libration dynamics and orbital perturbations of the mother satellite caused by the tether tension. Nagata [26] obtained solutions using thrusters on both the subsatellite and mother satellite to minimize a linear combination of the squares of the orbital deviations, libration angle, and fuel consumption. Solutions were obtained using direct collocation based on a fifth-degree Gauss–Lobatto transcription method. Fujii and Kojima [27] obtained symmetrical optimal deployment and retrieval trajectories to minimize the square of the velocity of the subsatellite using a geometrical approach. Stuart [28] obtained optimal trajectories for an in-plane tether-mediated rendezvous with a cooperative payload at the end of a nominal 10 km long tether. Stuart [28] considered both minimum fuel and maximum proximity time maneuvers using a gradient search algorithm.

Optimal deployment/retrieval trajectories have been studied previously for a small number of cases in which the tether has been treated as completely massless and inflexible. In most scenarios, deployment/retrieval profiles that satisfy the boundary conditions would seem to be suitable. However, such solutions are not unique and the question as to what performance index to employ when solving the optimal control problem remains open. In the literature, the cost function has typically been selected as either the integral square of the nondimensional tension or combinations of the square of the in-plane angle and the nondimensional tension, as described in the preceding paragraph. No physical basis for the selection of these cost functions has been given. Sometimes it is claimed that minimizing the tension is a measure of minimizing the control energy. In mechanical systems in which no active control is provided, the control input is typically zero. However, in tethered satellite systems, control actuation is achieved via variations in the tether length, which can be implemented indirectly by manipulating the tether tension at the deployer. Thus, even when the tether reel is locked, the tether tension can be quite significant. Furthermore, low tether tensions could be quite dangerous due to the increased risk of the tether becoming slack. For these reasons, the selection of an appropriate performance index to measure the optimality of the control system is considered important. One possible reason for the selection of the square of the tension in the performance index is that it allows the direct solution of the control variable when Pontryagin's maximum principle is applied. However, with the advent of sophisticated numerical methods, differentiability with respect to the control is no longer necessary. Thus, in this work, we seek to provide a benchmark and some physical reasoning for the selection of the cost function.

An issue of critical concern is the performance of the open-loop control law when applied to a flexible tether. This issue has been addressed in a preliminary fashion in Williams et al. [20], in which it was demonstrated that certain choices of the performance index give better performance of the control law when applied to a tether with flexibility. The purpose of this paper is to provide a comprehensive study of the effect of different performance indices on the optimal deployment and retrieval dynamics. In particular, comparisons of the open-loop trajectories for the cases in which the tether is inextensible and in which the tether can stretch longitudinally are provided. This provides a great deal of insight into selecting appropriate controllers to suppress the longitudinal vibration modes.

II. Mathematical Models

A two-body tethered satellite system consists of two satellites connected via a tether. The two satellites are assumed to be point masses and the tether connecting them is assumed to be straight (see Fig. 1). In addition, because deployment and retrieval do not generally take a large amount of time, the motion of the center of mass of the system is assumed to be an unperturbed Keplerian circular orbit. For simplicity, only the in-plane motion of the system is considered. Two cases may be considered for dynamical simulation: 1) the tether is treated as an inextensible rigid rod, and 2) the tether is treated as a longitudinally elastic spring. For the case in which the tether is assumed to be a spring, the strain is taken to be uniform along the tether length (see Fig. 1b). Note that this simplifies the analysis somewhat, but the nature of the results are still extremely insightful because they represent the fundamental mode of elastic vibration. The Lagrangians for both cases are similar and are stated below for completeness. For a rigid tether [10],

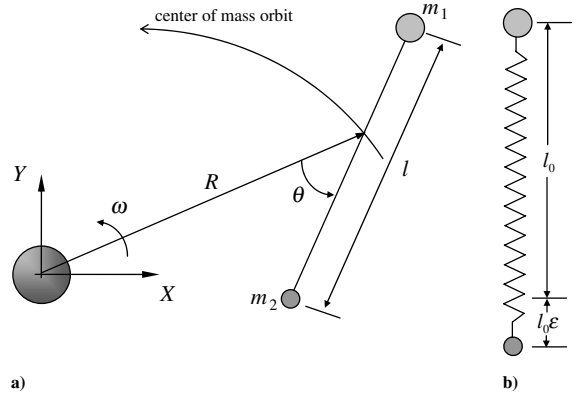

Fig. 1 Tethered satellite model: a) generalized coordinates, and b) representation of the tether longitudinal mode.

$$L_{\text{rigid}} = \tfrac{1}{2}m^* l^2(\dot{\theta}+\omega)^2 + \tfrac{1}{2}\bar{m}\dot{l}^2 - \tfrac{1}{2}m^* l^2\omega^2(1-3\cos^2\theta) \quad (1)$$

The Lagrangian for an elastic tether is similar but must be expressed in terms of the unstrained tether length and tether strain:

$$L_{\text{flexible}} = \frac{1}{2}m^* l_0^2(1+\varepsilon)^2(\dot{\theta}+\omega)^2 + \frac{1}{2}\bar{m}[\dot{l}_0(1+\varepsilon)+l_0\dot{\varepsilon}]^2 - \frac{1}{2}m^* l_0^2(1+\varepsilon)^2\omega^2(1-3\cos^2\theta) - \frac{EA}{2}l_0\varepsilon^2 \quad (2)$$

where $m^* = (m_1 + m_t/2)(m_2 + m_t/2)/m - m_t/6$ is the reduced system mass, $\bar{m} = m_1(m_2 + m_t)/m$, $m_1 = m_1^0 - m_t$ is the mother satellite mass, m_1^0 is the mother satellite mass before deployment of the tether, m_2 is the subsatellite mass, $m_t = \rho l_0$ is the deployed tether mass, ρ is the tether line density, θ is the in-plane libration angle, ω is the orbital angular velocity of the system center of mass, ε is the tether longitudinal strain, EA is the longitudinal tether stiffness, and l_0 is the unstrained tether length. Note that when the tether is treated as inextensible, the strain is zero and hence $l = l_0$. Figure 1b shows the way that tether strain is modeled in the case of an elastic tether.

A. Rigid Tether Equations

The equations of motion for a rigid tether may be derived by a straightforward application of Lagrange's equations:

$$\frac{\mathrm{d}}{\mathrm{d}t}\left(\frac{\partial L}{\partial \dot{q}_j}\right) - \frac{\partial L}{\partial q_j} = Q_{q_j} \quad (3)$$

The resulting equations of motion are obtained in nondimensional form as [10]

$$\theta'' + 2\frac{m_1(m_2+m_t/2)}{mm^*}\frac{\Lambda'}{\Lambda}(\theta'+1) + 3\sin\theta\cos\theta = 0 \quad (4)$$

$$\Lambda'' + \frac{(2m_1 - m)m_t}{2m_1(m_2 + m_t)}\frac{\Lambda'^2}{\Lambda} - \frac{(m_2 + m_t/2)}{m_2 + m_t}\Lambda[(\theta' + 1)^2 + (3\cos^2\theta - 1)] = -u \tag{5}$$

where $\Lambda = l/L_f$ is the nondimensional length, L_f is the reference length, $u = T/\{m_1(m_2 + m_t)\omega^2 L_f/m\}$ is the nondimensional tension control input, T is the tether control tension at the mother satellite, and $(\,)' = \mathrm{d}(\,)/\mathrm{d}(\omega t)$ is the nondimensional time derivative. Note that no other external forces except for gravity are assumed to act on the tether.

B. Elastic Tether Equations

Following in the same way for the elastic tether case, the nondimensional equations of motion for an elastic tether are obtained as

$$\theta'' + 2\left[\frac{m_1(m_2 + m_t/2)}{mm^*}\frac{\Lambda_0'}{\Lambda_0} + \frac{\varepsilon'}{1 + \varepsilon}\right](\theta' + 1) + 3\sin\theta\cos\theta = 0 \tag{6}$$

$$\varepsilon'' + \frac{\Lambda_0''}{\Lambda_0}(1 + \varepsilon) + 2\frac{\Lambda_0'}{\Lambda_0}\varepsilon' + \frac{(2m_1 - m)m_t}{m_1(m_2 + m_t)}\frac{\Lambda_0'}{\Lambda_0}\left[\frac{\Lambda_0'}{\Lambda_0}(1 + \varepsilon) + \varepsilon'\right] - \left[\frac{(m_1 + \frac{m_t}{3})(m_2 + \frac{m_t}{3}) - \frac{m_t^2}{36}}{m_1(m_2 + m_t)}\right](1 + \varepsilon)[(\theta' + 1)^2 + (3\cos^2\theta - 1)] = -\frac{EA}{L_f\Lambda_0\bar{m}\omega^2}\varepsilon \tag{7}$$

Although the general form of the equations of motion are similar between the rigid and elastic cases, it is evident that the equation of motion for the longitudinal strain is considerably more complex than Eq. (5) for the length variation of a rigid tether. Comparing Eq. (6) with Eq. (4) shows that the librational motion is perturbed only slightly by the longitudinal oscillations. The coupling means that structural damping in the tether can lead to some small damping of the tether librations over very long-term motions, as has been observed in the Tether Physics and Survivability mission. In addition, the well-known instabilities of the system when the length rate is negative ($\Lambda_0' < 0$) can be noted. However, because the system is nonlinear and coupled, variations in the length rate and length acceleration can be used to control both the longitudinal vibrations and the tether librations. This fact is exploited in this paper for the design of open-loop optimal trajectories.

C. Choice of Control Input

The method used to control the tether ultimately depends on the hardware used to implement a particular mission. For example, the TSS-1 mission used a reel deployer, whereas the small expendable deployer system (SEDS) employed a friction brake that controlled the tether tension as a function of the number of turns the tether made around a "barberpole." For the reference trajectory design, the choice of "control input" is dictated by the available mathematical model. For example, when an inelastic model is used, the logical choice is tether tension because it is straightforward to implement appropriate physical bounds on the tether tension via the control input. Knowledge of the tether tension can be used to change the control input to another variable of choice, such as reel rate, or the reel acceleration using the same model. Hence, the trajectory design and the final implementation of the control can be effectively decoupled. The use of reel rate as a control for trajectory design is not a straightforward choice due to the difficulties in ensuring that constraints on the tether tension are met in the nominal design. Furthermore, the reel rate must remain continuous, which makes other inputs such as reel acceleration or tension more appropriate. For the elastic tether model, tension cannot be used directly. Instead, the second derivative of the unstrained tether length is used. This selection is again based on the dynamic equations, for which this term appears in the strain equation. In other words, because the elastic equations include longitudinal dynamics, it is no longer appropriate to control the tension directly. Instead, control of the unstrained length is more appropriate. At this point, it should be clear that the inelastic model, although less accurate, enables a wider choice of "controls" at the expense of neglecting longitudinal dynamics. It should also be apparent that the control input used for the design of trajectories does not necessarily translate into the physical control input used in a final system. Hence, although tension control is employed for the rigid tether control design, this is purely open loop and can be further translated into any other desirable control parameter to be implemented in a mission.

III. Optimal Deployment and Retrieval Trajectories

A. Measures of Optimality for Tethered Satellite Deployment and Retrieval

As mentioned previously, the only control actuation assumed to be available for the tethered satellite system is changes in tether length. In the rigid tether case, the control input is taken to be the nondimensional tether tension, whereas in the case of an elastic tether, it is taken to be the nondimensional reel acceleration. It is often the case that a performance index is employed that is quadratic in the controls. For example, for optimal control of a rigid tether, a performance index quadratic in the tether tension has been used many times. This is despite the fact that there is no good reason why the tension should be minimized. This is somewhat similar to the growing anomaly of engineers applying quadratic performance indices (in the thrust) to spacecraft control problems, which is known to give non-fuel-optimal trajectories [29].

There are several performance characteristics of the tethered system that might be considered as potential quantities to be optimized during deployment and retrieval. For example, the work done by the tether reel or the tether reel rate may want to be kept as low as possible. For the most part, the cost function selection may need to be tailored for each specific mission. However, the aim of this paper is to provide some general guidelines and recommendations that should aid in this selection. The performance indices considered in this paper are described in the following subsections. Note, there are an infinite number of possible performance measures that can be used in optimal control problems. To focus on the essential nature of the dynamics, only individual performance measures are considered. That is, weighted combinations of different costs are not considered. However, the information provided by each component alone provides a great deal of insight into the applicability of such weighted costs.

The performance indices selected for comparison are summarized in Table 1 for the case of a rigid tether and Table 2 for the case of an elastic tether. Similar performance measures were selected whenever possible so as to compare the results for rigid and elastic tethers. The first measure selected is minimum tension. Although there is no good physical basis for selecting a minimum tension performance index, it is included in this study because of its prior use and to compare its performance relative to other performance measures. For a rigid tether, the cost function can be defined purely in terms of the control input ($\mathcal{J}_1^r$, Table 1), whereas for an elastic tether, minimum tension is equivalent to minimum strain ($\mathcal{J}_1^e$, Table 2). The use of a quadratic performance index leads to continuous control inputs. Minimum tension may also be defined in an l_1-optimal sense ($\mathcal{J}_2^r$, Table 1) because the tension is constrained to be nonnegative, $u > 0$, to prevent the tether from becoming slack.

One of the major problems faced by tethered satellite systems is the possibility of a slack tether. When the tether length is short, the gravity-gradient forces on the system are very small and hence the tether tension is very low. This poses potential problems during the terminal stages of retrieval and the early stages of deployment. In light of this, one possible performance measure is to maximize the tether tension ($\mathcal{J}_3^r$, Table 1), maximize the l_1 norm of the tension ($\mathcal{J}_4^r$, Table 1), or maximize the tether strain for an elastic tether ($\mathcal{J}_2^e$, Table 2).

In general, we are more interested in the tether dynamics being well behaved than in minimizing a functional of the tether tension. In

Table 1 Performance measures for the rigid tether

Label	Measure	Performance index	Physical reasoning
$\mathcal{J}_1^r$	Minimum tension	$\int_{\tau_0}^{\tau_f} u^2 \, d\tau$	Minimum "control" energy
$\mathcal{J}_2^r$	Minimum l_1 tension	$\int_{\tau_0}^{\tau_f} u \, d\tau$	Minimum control energy in l_1-norm sense
$\mathcal{J}_3^r$	Maximum tension	$-\int_{\tau_0}^{\tau_f} u^2 \, d\tau$	Try to maximize the tension to prevent slackness
$\mathcal{J}_4^r$	Maximum l_1 tension	$-\int_{\tau_0}^{\tau_f} u \, d\tau$	Try to maximize the tension in l_1-norm sense to prevent slackness
$\mathcal{J}_5^r$	Minimum tension rate	$\int_{\tau_0}^{\tau_f} (u')^2 \, d\tau$	Minimize the likelihood of induced longitudinal vibrations
$\mathcal{J}_6^r$	Minimum power	$\int_{\tau_0}^{\tau_f} (\Lambda' u \frac{m_1(m_2+m_t)}{m} \omega)^2 \, d\tau$	Minimize the amount of work required by the reel mechanism
$\mathcal{J}_7^r$	Minimum libration angle	$\int_{\tau_0}^{\tau_f} \theta^2 \, d\tau$	Try to prevent large excursions of the tether; prevent collisions with spacecraft structure
$\mathcal{J}_8^r$	Minimum libration rate	$\int_{\tau_0}^{\tau_f} \theta'^2 \, d\tau$	Try to prevent large swing rates to minimize adverse effects of a deployment jam
$\mathcal{J}_9^r$	Minimum libration acceleration	$\int_{\tau_0}^{\tau_f} (\theta'')^2 \, d\tau$	Minimize the angular acceleration of the tether to maintain smoother swing dynamics
$\mathcal{J}_{10}^r$	Minimum length rate	$\int_{\tau_0}^{\tau_f} \Lambda'^2 \, d\tau$	Minimize the amount of reeling required
$\mathcal{J}_{11}^r$	Minimum length acceleration	$\int_{\tau_0}^{\tau_f} (\Lambda'')^2 \, d\tau$	Minimize how fast the reel rate needs to be adjusted so as to maintain a smooth deployment profile
$\mathcal{J}_{12}^r$	Minimum tension acceleration	$\int_{\tau_0}^{\tau_f} (u'')^2 \, d\tau$	Try minimize changes in the tension rate to prevent large longitudinal vibrations
$\mathcal{J}_{13}^r$	Minimum time	τ_f	Obtain the fastest possible deployment
$\mathcal{J}_{14}^r$	Minimax libration angle	$\max \lvert\theta\rvert$	Minimize the maximum observed libration angle to prevent the tether colliding with spacecraft structure
$\mathcal{J}_{15}^r$	Minimax libration rate	$\max \lvert\theta'\rvert$	Minimize the maximum observed swing rate
$\mathcal{J}_{16}^r$	Minimax libration acceleration	$\max \lvert\theta''\rvert$	Minimize the maximum observed swing acceleration
$\mathcal{J}_{17}^r$	Minimax length rate	$\max \lvert\Lambda'\rvert$	Minimize the maximum observed reel rate
$\mathcal{J}_{18}^r$	Minimax length acceleration	$\max \lvert\Lambda''\rvert$	Minimize the maximum observed reel acceleration
$\mathcal{J}_{19}^r$	Minimax tension	$\max \lvert u\rvert$	Minimize the maximum observed tension to prevent tether severance
$\mathcal{J}_{20}^r$	Minimax tension rate	$\max \lvert u'\rvert$	Minimize the maximum observed tension rate to reduce longitudinal oscillations
$\mathcal{J}_{21}^r$	Minimax tension acceleration	$\max \lvert u''\rvert$	Minimize the maximum observed change in tension rate to reduce longitudinal oscillations

Table 2 Performance measures for elastic tether

Label	Measure	Performance index	Physical reasoning
$\mathcal{J}_1^e$	Minimum strain	$\int_{\tau_0}^{\tau_f} (\varepsilon)^2 \, d\tau$	To obtain equivalent of minimum control energy trajectory
$\mathcal{J}_2^e$	Maximum strain	$-\int_{\tau_0}^{\tau_f} (\varepsilon)^2 \, d\tau$	Maximize tether tension to prevent tether slackness
$\mathcal{J}_3^e$	Minimum tension rate	$\int_{\tau_0}^{\tau_f} (EA\varepsilon')^2 \, d\tau$	Minimize the induced tether longitudinal vibrations
$\mathcal{J}_4^e$	Minimum power	$\int_{\tau_0}^{\tau_f} (EA\varepsilon \dot{l}_0)^2 \, d\tau$	Minimize the amount of work performed by the reel
$\mathcal{J}_5^e$	Minimum libration angle	$\int_{\tau_0}^{\tau_f} \theta^2 \, d\tau$	Try to prevent large excursions of the tether; prevent collisions with spacecraft structure
$\mathcal{J}_6^e$	Minimum libration rate	$\int_{\tau_0}^{\tau_f} \theta'^2 \, d\tau$	Try to prevent large swing rates to minimize adverse effects of a deployment jam
$\mathcal{J}_7^e$	Minimum libration acceleration	$\int_{\tau_0}^{\tau_f} (\theta'')^2 \, d\tau$	Minimize the angular acceleration of the tether to maintain smoother swing dynamics
$\mathcal{J}_8^e$	Minimum strained length rate	$\int_{\tau_0}^{\tau_f} [\Lambda_0'(1+\varepsilon) + \Lambda_0\varepsilon']^2 \, d\tau$	Minimize the amount of combined reeling and induced longitudinal vibrations
$\mathcal{J}_9^e$	Minimum unstrained length rate	$\int_{\tau_0}^{\tau_f} [\Lambda_0']^2 \, d\tau$	Minimize the amount of reeling required
$\mathcal{J}_{10}^e$	Minimum strained length acceleration	$\int_{\tau_0}^{\tau_f} [\Lambda_0''(1+\varepsilon) + 2\Lambda_0'\varepsilon' + \Lambda_0\varepsilon'']^2 \, d\tau$	Minimize total radial acceleration of the payload; combined reel acceleration and induced longitudinal accelerations
$\mathcal{J}_{11}^e$	Minimum unstrained length acceleration	$\int_{\tau_0}^{\tau_f} (\Lambda_0'')^2 \, d\tau$	Minimize how fast the reel rate needs to be adjusted so as to maintain a smooth deployment profile; minimum control energy for elastic tether
$\mathcal{J}_{12}^e$	Minimum strain acceleration	$\int_{\tau_0}^{\tau_f} (\varepsilon'')^2 \, d\tau$	Try to minimize changes in the strain rate to prevent large longitudinal vibrations
$\mathcal{J}_{13}^e$	Minimum time	τ_f	Obtain the fastest possible deployment
$\mathcal{J}_{14}^e$	Minimax libration angle	$\max \lvert\theta\rvert$	Minimize the maximum observed libration angle to prevent the tether colliding with spacecraft structure
$\mathcal{J}_{15}^e$	Minimax libration rate	$\max \lvert\theta'\rvert$	Minimize the maximum observed swing rate
$\mathcal{J}_{16}^e$	Minimax libration acceleration	$\max \lvert\theta''\rvert$	Minimize the maximum observed swing acceleration
$\mathcal{J}_{17}^e$	Minimax strained length rate	$\max \lvert\Lambda_0'(1+\varepsilon) + \Lambda_0\varepsilon'\rvert$	Minimize the maximum observed total length rate (combined strain rate and deployment rate)
$\mathcal{J}_{18}^e$	Minimax unstrained length rate	$\max \lvert\Lambda_0'\rvert$	Minimize the maximum observed deployment rate
$\mathcal{J}_{19}^e$	Minimax strained length acceleration	$\max \lvert\Lambda_0''(1+\varepsilon) + 2\Lambda_0'\varepsilon' + \Lambda_0\varepsilon''\rvert$	Minimize the maximum observed total length acceleration (combined strain acceleration and reel acceleration)
$\mathcal{J}_{20}^e$	Minimax unstrained length acceleration	$\max \lvert\Lambda_0''\rvert$	Minimize the maximum observed reel acceleration
$\mathcal{J}_{21}^e$	Minimax strain	$\max \lvert\varepsilon\rvert$	Minimize the maximum observed strain to prevent tether severance
$\mathcal{J}_{22}^e$	Minimax strain rate	$\max \lvert\varepsilon'\rvert$	Minimize the maximum observed strain rate
$\mathcal{J}_{23}^e$	Minimax strain acceleration	$\max \lvert\varepsilon''\rvert$	Minimize the maximum observed change in change rate

particular, one may want to avoid sudden *changes* in the tether tension that could lead to large amplitude vibrations in the flexible tether modes. To minimize the tension rate for a rigid tether requires the introduction of a new state variable, representing the tether tension, and the new control variable becomes the tension rate (u_*), that is, $u' = u_*$, ($\mathcal{J}_5^r$, Table 1). For an elastic tether, minimizing the tension rate is equivalent to minimizing the strain rate ($\mathcal{J}_3^e$, Table 2). In other words, for an elastic tether we can use the elastic vibrations within the cost function to penalize the longitudinal dynamics. One would expect different responses for the rigid and elastic tethers, in general, because penalizing the tension variation in a rigid tether only focuses on the long-term variations in tension due to changes in length and the effect of the gravity gradient, whereas an elastic tether is subject to both short-period and long-period variations in tension.

The power used by the tether reel system is, in general, a better indicator of control performance than the tether tension. For a rigid tether, the instantaneous power used by the reel may be expressed as

$$P = \Lambda' u \frac{m_1(m_2 + m_t)}{m} \omega^3 L_f^2 \tag{8}$$

leading to the cost shown as $\mathcal{J}_6^r$ in Table 1. For an elastic tether, the power is defined in terms of the unstrained tether length rate ($\mathcal{J}_4^e$, Table 2).

There may be circumstances in which the deviations of particular state variables, such as the libration angle, may want to be kept small. For example, if deployment from a large space structure such as a space station is to be undertaken, it may be desirable to try to minimize the potential for contact with the structure, which would include minimizing the excursion of the tether in the direction of the local horizon ($\mathcal{J}_7^r$, Table 1; $\mathcal{J}_5^e$, Table 2).

Instead of minimizing the libration angle directly, it may be appropriate to minimize the libration rate ($\mathcal{J}_8^r$, Table 1; $\mathcal{J}_6^e$, Table 2) or librational acceleration ($\mathcal{J}_9^r$, Table 1; $\mathcal{J}_7^e$, Table 2). These cost functions may be useful for preventing large excursions of the tether angle in the case in which the deployment jams in flight. Similarly, the minimization of the angular acceleration of the tether might also be a good potential performance index because it is directly related to the control actuation provided by variations in tether length.

The control of the tether librations is achieved only indirectly via the tether length rate and hence the controller may attempt to apply relatively large length rates to achieve its objectives. This is undesirable from a practical point of view because there are maximum reel-rate restrictions on all reel mechanisms. To keep the reel rate low, the tether reel rate can be minimized ($\mathcal{J}_{10}^r$, Table 1). For an elastic tether, the equivalent length rate is the total length rate that involves both the unstrained length rate and strain rate ($\mathcal{J}_8^e$, Table 2). Alternatively, the unstrained length rate can be minimized ($\mathcal{J}_9^e$, Table 2).

One of the key requirements for an elastic tether is that the dynamics remain "well behaved." Sudden changes in the deployment rate can lead to oscillations in the flexible modes and hence it is desirable to try to keep the deployment dynamics as smooth as possible. For this reason, minimizing the length acceleration may be a very good performance measure ($\mathcal{J}_{11}^r$, Table 1). Again, for an elastic tether, either the total length acceleration ($\mathcal{J}_{10}^e$, Table 2) or the unstrained length acceleration ($\mathcal{J}_{11}^e$, Table 2) can be used. Note that the unstrained length acceleration is the control input for the elastic tether model.

If the longitudinal vibrations are considered to be of most importance, minimizing the strain acceleration should lead to smoother variations in the strain rate ($\mathcal{J}_{12}^e$, Table 2). The counterpart for a rigid tether would be the tension acceleration. To minimize the tension acceleration for a rigid tether requires the introduction of two new state variables, representing the tether tension and tension rate, and the new control variable becomes the tension acceleration, that is, $u'' = u_*$, ($\mathcal{J}_{12}^r$, Table 1).

An important class of solutions for deployment and retrieval are those that belong to minimum time cost functions. Time optimal control solutions are generally of a bang–bang nature, but are important because they set the lower bound on achievable deployment/retrieval time ($\mathcal{J}_{13}^r$, Table 1; $\mathcal{J}_{13}^e$, Table 2).

In addition to forming lower bounds on the deployment and retrieval times, bounds on various other performance parameters can be established by solving minimax optimal control problems for various functions. For example, we can compare the performance of different controllers relative to the minimax performance. Minimax functionals have been formed for each of the key dynamic variables: libration angle ($\mathcal{J}_{14}^r$, Table 1; $\mathcal{J}_{14}^e$, Table 2), libration rate ($\mathcal{J}_{15}^r$, Table 1; $\mathcal{J}_{15}^e$, Table 2), libration acceleration ($\mathcal{J}_{16}^r$, Table 1; $\mathcal{J}_{16}^e$, Table 2), length rate ($\mathcal{J}_{17}^r$, Table 1), total length rate ($\mathcal{J}_{17}^e$, Table 2) and unstrained length rate ($\mathcal{J}_{18}^e$, Table 2) for an elastic tether, length acceleration ($\mathcal{J}_{18}^r$, Table 1), total length acceleration ($\mathcal{J}_{19}^e$, Table 2) and unstrained length acceleration ($\mathcal{J}_{20}^e$, Table 2) for an elastic tether, tension ($\mathcal{J}_{19}^r$, Table 1) or strain ($\mathcal{J}_{21}^e$, Table 2) for an elastic tether, tension rate ($\mathcal{J}_{20}^r$, Table 1) or strain rate ($\mathcal{J}_{22}^e$, Table 2) for an elastic tether, tension acceleration ($\mathcal{J}_{21}^r$, Table 1) or strain acceleration ($\mathcal{J}_{23}^e$, Table 2) for an elastic tether.

B. Boundary Conditions

The local vertical direction is typically the desired orientation for a tethered system during deployment and retrieval. However, because of gravity-gradient effects and a rotating orbital frame, changes in tether length cause the tether to move away from the local vertical. In fact, if the length rate is too excessive then the entire tether system can begin rotating. This is undesirable for the type of applications considered here and so appropriate boundary conditions must be specified to fully describe the optimal control problem and to prevent such occurrences. There are certain boundary conditions that must be given to specify whether the problem is deployment or retrieval. For example, the initial and final tether length must be set. In some circumstances, some of the initial conditions could serve as potential optimization parameters. For example, the ejection angle and ejection speed during deployment could be useful parameters to optimize.

In this study, the nominal boundary conditions are set as

$$[\theta, \theta', \Lambda, \Lambda']_{\tau=0} = [0, 0, 0.1, 0], \qquad [\theta, \theta', \Lambda, \Lambda']_{\tau=\tau_f} = [0, 0, 1, 0] \tag{9}$$

for a rigid tether. For an elastic tether, we demand that the extended tether length be equal to the desired length so that the boundary conditions are

$$\begin{aligned} &[\theta, \theta', \varepsilon, \varepsilon', \Lambda_0, \Lambda_0']_{\tau=0} = [0, 0, \varepsilon_0, 0, 0.1, 0], \\ &[\theta, \theta', \Lambda_0(1+\varepsilon), \varepsilon', \Lambda_0']_{\tau=\tau_f} = [0, 0, 1, 0, 0] \end{aligned} \tag{10}$$

Note the nonlinear final boundary condition for the extended tether length, $\Lambda_0(1+\varepsilon)$ rather than simply Λ_0. The initial tether strain is set so that the initial tether strain acceleration is zero:

$$\varepsilon(\tau_0) = \left. \frac{\left[\frac{(m_1+\frac{m_t}{3})(m_2+\frac{m_t}{3})-\frac{m_t^2}{36}}{m_1(m_2+m_t)}\right][(\theta'+1)^2 + (3\cos^2\theta - 1)] - \frac{(2m_1-m)m_t}{m_1(m_2+m_t)}\frac{\Lambda_0'}{\Lambda_0}\frac{\Lambda_0'}{\Lambda_0}}{\frac{(2m_1-m)m_t}{m_1(m_2+m_t)}\frac{\Lambda_0'}{\Lambda_0}\frac{\Lambda_0'}{\Lambda_0} + \frac{EA}{L_f\Lambda_0\bar{m}\omega^2} - \left[\frac{(m_1+\frac{m_t}{3})(m_2+\frac{m_t}{3})-\frac{m_t^2}{36}}{m_1(m_2+m_t)}\right][(\theta'+1)^2 + (3\cos^2\theta - 1)]} \right|_{\tau_0} \tag{11}$$

which is evaluated for the initial tether parameters. The effects of the nonzero initial libration angle and different initial lengths are studied later.

Additional boundary conditions have also been considered. For example, the nominal boundary conditions ensure that the length rate is zero at the final time, but this does not ensure that the final length acceleration is zero. However, this additional constraint simply results in the tension jumping to the value required for equilibrium and is not considered in the numerical results in this paper.

C. State and Control Constraints

One of the most important constraints that must be enforced for a tethered satellite system is that the tether always retains positive tension. This is obvious because a wire or string cannot sustain compression forces, in general. Slack tethers are undesirable from a control point of view because it may be very difficult to regain control of the subsatellite without using thrusters or some other form of control input. To ensure that the tether remains taut, the following control constraint is used for the rigid tether model

$$T_{\min} \le u\frac{m_1(m_2+m_t)}{m}\omega^2 L_f \le T_{\max} \tag{12}$$

Note that if the tether mass is neglected, then Eq. (12) is independent of the system state variables, whereas if the mass variation of the system is taken into account, then Eq. (12) is a mixed state-control constraint. Note that an upper bound is placed on the tension to prevent the tether from breaking.

For an elastic tether, the tension constraint is enforced as a linear state constraint

$$T_{\min} \le EA\varepsilon \le T_{\max} \Leftrightarrow T_{\min}/EA \le \varepsilon \le T_{\max}/EA \tag{13}$$

The tension constraint is the minimum constraint that must be enforced. Additional state constraints, such as on the tether reel rate, may also be employed. A practical constraint on the tether reel rate can arise through the use of SEDS-type braking deployers, which only allow the tether to be reeled out. This introduces the state constraint

$$\Lambda' \ge 0, \qquad \Lambda'_0 \ge 0 \tag{14}$$

Because of space limitations, this constraint will not be considered in the numerical results.

D. Symmetry of Deployment and Retrieval

One important result that will be stated formally in this paper is related to the symmetry present in the deployment and retrieval trajectories. The deployment/retrieval symmetry theorem has been observed previously in numerical computations for inelastic tethers [10,27]. This section demonstrates that the symmetry is also present for elastic tethers. For the purposes of this study, the proof is extremely important because it means that the computation of a deployment trajectory automatically implies a feasible retrieval trajectory that generates the same cost function value. The important restriction is that the initial and terminal boundary conditions for deployment are the terminal and initial boundary conditions for retrieval, respectively. Therefore, we have immediately halved the amount of computation necessary for comparing the different cost functions considered in this paper.

1. Inextensible Tether

Theorem 1: Suppose there exists a deployment trajectory $\theta_d(\tau)$, $\theta'_d(\tau)$, $\Lambda_d(\tau)$, $\Lambda'_d(\tau)$, $u_d(\tau)$ satisfying the initial conditions $\theta_d(\tau_0)=\theta_0$, $\theta'_d(\tau_0)=\theta'_0$, $\Lambda_d(\tau_0)=\Lambda_0$, $\Lambda'_d(\tau_0)=\Lambda'_0$ and the final conditions $\theta_d(\tau_f)=\theta_f$, $\theta'_d(\tau_f)=\theta'_f$, $\Lambda_d(\tau_f)=\Lambda_f$, $\Lambda'_d(\tau_f)=\Lambda'_f$, then there exists a retrieval trajectory satisfying the initial conditions $\theta_r(\tau_0)=-\theta_f$, $\theta'_r(\tau_0)=\theta'_f$, $\Lambda_r(\tau_0)=\Lambda_f$, $\Lambda'_r(\tau_0)=-\Lambda'_f$ and the final conditions $\theta_r(\tau_f)=-\theta_0$, $\theta'_r(\tau_f)=\theta'_0$, $\Lambda_r(\tau_f)=\Lambda_0$, $\Lambda'_r(\tau_f)=-\Lambda'_0$ given by $\theta_r(\tau)=-\theta_d(\tau_f-\tau)$, $\theta'_r(\tau)=\theta'_d(\tau_f-\tau)$, $\Lambda_r(\tau)=\Lambda_d(\tau_f-\tau)$, $\Lambda'_r(\tau)=-\Lambda'_d(\tau_f-\tau)$, $u_r(\tau)=u_d(\tau_f-\tau)$.

Proof: The proof is relatively straightforward. If one substitutes the retrieval trajectory into Eqs. (4) and (5), then

$$\theta''_r = 2f_1(\Lambda_d(\tau_f-\tau))\frac{\Lambda'_d(\tau_f-\tau)}{\Lambda_d(\tau_f-\tau)}(\theta'_d(\tau_f-\tau)+1) + 3\sin\theta_d(\tau_f-\tau)\cos\theta_d(\tau_f-\tau) = -\theta''_d(\tau_f-\tau) \tag{15}$$

$$\Lambda''_r = -f_2(\Lambda_d(\tau_f-\tau))\frac{\Lambda'_d(\tau_f-\tau)^2}{\Lambda_d(\tau_f-\tau)} + f_3(\Lambda_d(\tau_f-\tau))\Lambda_d(\tau_f-\tau)[(\theta'_d(\tau_f-\tau)+1)^2 + (3\cos^2\theta_d(\tau_f-\tau)-1)] - u_d(\tau_f-\tau) = \Lambda''_d(\tau_f-\tau) \tag{16}$$

Thus, an integration with respect to $-\tau$ must yield the deployment trajectory but with a negative reel rate and negative libration angle. This is the retrieval trajectory. Note that this is only true for symmetric boundary conditions.

2. Elastic Tether

For the case of an elastic tether, we must account for the tether strain as well as the tether length variations. However, the theorem is basically the same as the rigid tether case and is omitted for the sake of brevity. The result is that an integration of the equations of motion with respect to $-\tau$, with symmetric boundary conditions, yields the deployment trajectory, but with a negative strain rate and negative libration angle. This is the retrieval trajectory.

Remarks: Symmetry of deployment/retrieval is only true of the reference trajectory determination. It does not apply to the true dynamic behavior of a tether subjected to perturbations. This fact has been well established in the literature on tethered satellites [9,13], for which significant instability is present during retrieval. The instability is due to the presence of $\dot{l}/l$ (or Λ'/Λ) in the libration and elastic equations. This term removes energy during deployment and adds energy during retrieval. Hence, feedback control around the reference trajectories is very different between the two cases. Retrieval is inherently unstable. In addition, any strategy that relies on the direct numerical integration of the equations of motion for developing an optimal retrieval trajectory will also be similarly plagued by instabilities due to the sensitivity of the system to variations in initial conditions. The symmetry theorem presented here shows that this is unnecessary, because a forward simulation of deployment with the appropriate transformation of variables establishes the reference trajectories for retrieval. After a reference trajectory has been selected, the design of a feedback control strategy is required. Control of retrieval with flexible tethers is still considered a very challenging problem.

E. Out-of-Plane Effects

The results in this paper are limited to the in-plane motion only. When out-of-plane motion is present, length rate actuation is insufficient to completely eliminate the out-of-plane component in the short term. This also makes retrieval with out-of-plane motion more difficult than deployment. Hence, an additional actuator such as a thruster or electromagnetic forces may be required.

IV. Numerical Method

The general family of optimal control problems considered in this paper can be stated as follows. Find the controls $\boldsymbol{u}(t)$ and vector of parameters $\boldsymbol{p}$ that minimize the performance index:

$$\mathcal{J} = \mathcal{E}[\boldsymbol{x}(t_f), \boldsymbol{p}, t_f] + \int_{t_0}^{t_f} \mathcal{L}[\boldsymbol{x}(t), \boldsymbol{u}(t), \boldsymbol{p}, t]\,\mathrm{d}t \tag{17}$$

subject to the nonlinear state equations

$$\dot{\boldsymbol{x}}(t) = \boldsymbol{f}(\boldsymbol{x}(t), \boldsymbol{u}(t), \boldsymbol{p}, t) \tag{18}$$

the end point conditions

$$\boldsymbol{e}_L^0 \le \boldsymbol{e}[\boldsymbol{x}(t_0), t_0] \le \boldsymbol{e}_U^0 \tag{19}$$

$$\boldsymbol{e}_L^f \le \boldsymbol{e}[\boldsymbol{x}(t_f), t_f] \le \boldsymbol{e}_U^f \tag{20}$$

path constraints

$$\boldsymbol{g}_L \le \boldsymbol{g}[\boldsymbol{x}(t), \boldsymbol{u}(t), \boldsymbol{p}, t] \le \boldsymbol{g}_U \tag{21}$$

and box constraints

$$\boldsymbol{x}_L \le \boldsymbol{x}(t) \le \boldsymbol{x}_U \qquad \boldsymbol{u}_L \le \boldsymbol{u}(t) \le \boldsymbol{u}_U \qquad \boldsymbol{p}_L \le \boldsymbol{p} \le \boldsymbol{p}_U \tag{22}$$

where $\boldsymbol{x} \in \mathbb{R}^{n_x}$ are the state variables, $\boldsymbol{u} \in \mathbb{R}^{n_u}$ are the control inputs, $\boldsymbol{p} \in \mathbb{R}^{n_p}$ are a set of additional optimization parameters, $t \in \mathbb{R}$ is the time, $\mathcal{E}$: $\mathbb{R}^{n_0} \times \mathbb{R}^{n_p} \times \mathbb{R} \to \mathbb{R}$ is the Mayer cost function, $\mathcal{L}$: $\mathbb{R}^{n_x} \times \mathbb{R}^{n_u} \times \mathbb{R}^{n_p} \times \mathbb{R} \to \mathbb{R}$ is the integrand of the Bolza cost function, $\boldsymbol{e}_L^0 \in \mathbb{R}^{n_x} \times \mathbb{R} \to \mathbb{R}^{n_0}$ and $\boldsymbol{e}_U^0 \in \mathbb{R}^{n_x} \times \mathbb{R} \to \mathbb{R}^{n_0}$ are the lower and upper bounds on the initial point conditions, $\boldsymbol{e}_L^f \in \mathbb{R}^{n_x} \times \mathbb{R} \to \mathbb{R}^{n_f}$ and $\boldsymbol{e}_U^f \in \mathbb{R}^{n_x} \times \mathbb{R} \to \mathbb{R}^{n_f}$ are the lower and upper bounds on the final point conditions, and $\boldsymbol{g}_L \in \mathbb{R}^{n_x} \times \mathbb{R}^{n_u} \times \mathbb{R}^{n_p} \times \mathbb{R} \to \mathbb{R}^{n_g}$ and $\boldsymbol{g}_U \in \mathbb{R}^{n_x} \times \mathbb{R}^{n_u} \times \mathbb{R}^{n_p} \times \mathbb{R} \to \mathbb{R}^{n_g}$ are the lower and upper bounds on the path constraints. The solution of general optimal control problems requires the application of Pontryagin's maximum principle to construct the necessary conditions for optimality. This (indirect) approach, apart from being cumbersome for complex problems, produces a two-point boundary value problem that is regarded as being very difficult to solve [30]. In addition to this, the necessary conditions must be rederived for each different cost function that is considered. Instead of following this approach, it is much more efficient and convenient to apply direct transcription methods to solve the optimal control problem [31].

A. Minimax Optimal Control

An important class of optimal control problems are those belonging to the minimization of the maximum occurrence of a particular quantity, or minimax optimal control. A minimax optimal control problem can be reformulated so that it can be solved within the aforementioned framework. First, consider the problem of finding the controls $\boldsymbol{u}(t)$ to minimize

$$\mathcal{J} = \max F(\boldsymbol{x}(t), \boldsymbol{u}(t), t) \tag{23}$$

subject to Eqs. (18–22), where F: $\mathbb{R}^{n_x} \times \mathbb{R}^{n_u} \times \mathbb{R} \to \mathbb{R}$. This problem may be converted to a standard constrained optimal control problem by minimizing the unknown parameter p subject to the additional path constraint

$$F(\boldsymbol{x}(t), \boldsymbol{u}(t), t) - p \le 0 \tag{24}$$

In the case in which the maximum absolute value of F is to be minimized, the additional path constraint must be added to the formulation

$$-F(\boldsymbol{x}(t), \boldsymbol{u}(t), t) - p \le 0 \tag{25}$$

B. Direct Solution Methods

The solution of optimal control problems via direct methods is well known and several different methods are described in Betts [31]. There are a wide variety of solution methods available, most of which are based on sequential quadratic programming algorithms for solving the underlying nonlinear programming problem (NLP). Essentially, the state equations and cost function are discretized at a set of points along the trajectory, and the state equations are enforced through simple integration or differentiation rules. Although the general methodology involved with each method is the same, the underlying structure of the NLP and corresponding solution accuracy can be quite different.

Two discretizations are used to solve the optimal control problems in this paper: the Hermite–Simpson method [32] and the Legendre pseudospectral method [33,34]. The DIRECT [35] software is used to automate the implementation of these methods. The NLP generated by DIRECT is solved using the sparse sequential quadratic programming software SNOPT [36], originally coded in Fortran but called from MATLAB via a MEX-file interface.

V. Numerical Results

To examine the effect of the various cost functions on the optimal deployment and retrieval dynamics, a baseline system configuration is used. Parametric studies of the effect of different end masses, tether density, orbital altitude, and so on are considered for some, but not all, cost functions. The major focus of this study is to examine the effect of different formulations of the optimal control problem on the dynamics of a tethered satellite system. The nominal configuration selected to perform the comparison is given in Table 3. Results for deployment are given for the rigid tether case first, then results from the elastic tether case follow. All numerical results were generated using 200 nodes for the discretization. The optimal solutions were verified by propagating the interpolated controls using `ode45` in MATLAB.

A. Inelastic Tether

1. Nominal Trajectories

Numerical results for minimum tension, minimum l_1 tension, and maximum tension (both l_2 and l_1) are shown in Fig. 2. Here we can see the dramatic influence that the performance index has on the system trajectories. For minimum tension, the tension is kept as low as possible at the beginning of deployment when the natural tension is low because of the short tether length. This causes the tether to be reeled in slightly, and its length to be kept nearly constant. After roughly 0.4 of an orbit, the tether is reeled out rapidly to meet the length constraint at the final time. Note that there is slight pause in the deployment to allow the tether to swing back to the local vertical. It is interesting to note the dramatic differences between minimizing the l_2 and l_1 norm of the tension. Although there is some similarity in the variation in length, the tension history and corresponding librational dynamics are very different than the l_2 norm case. In particular, the tension is on the lower bound for the majority of the deployment, with three major peaks in the terminal stages of the deployment. The maximum tension deployment trajectories show similar undesirable features in the tension and length. Because the tether tension is linearly related to the tether length, maximizing the tension leads to a scenario in which the tether is significantly overdeployed (approximately 78 km of extra tether would be needed). To achieve this, the tension is initially set on the lower bound to allow the tether length to increase rapidly. The tension is then set to the upper bound for a significant period of time. The result is a trajectory that would be highly unstable, as can be seen from the "wandering" of the subsatellite in the trajectory plot in Fig. 2. Although the results are presented in nondimensional form, for the scenario considered here, 1 unit of nondimensional length rate corresponds to approximately 110.7 m/s in dimensional units. Thus, all three of these trajectories require some significant reel-rate requirements. In fact, the maximum tension trajectory requires the largest reel rate of all the trajectories considered in this paper (175 m/s).

Table 3 Basic parameters for tethered satellite system

Parameter	Value
Mother satellite mass, m_1^0	5000 kg
Subsatellite mass, m_2	500 kg
Orbital altitude	500 km
Minimum tether tension	0.2 N
Maximum tether tension	400 N
Deployed reference length, L_f	100 km
Tether line density, ρ	1 kg/km
Tether stiffness, EA	60,000 N

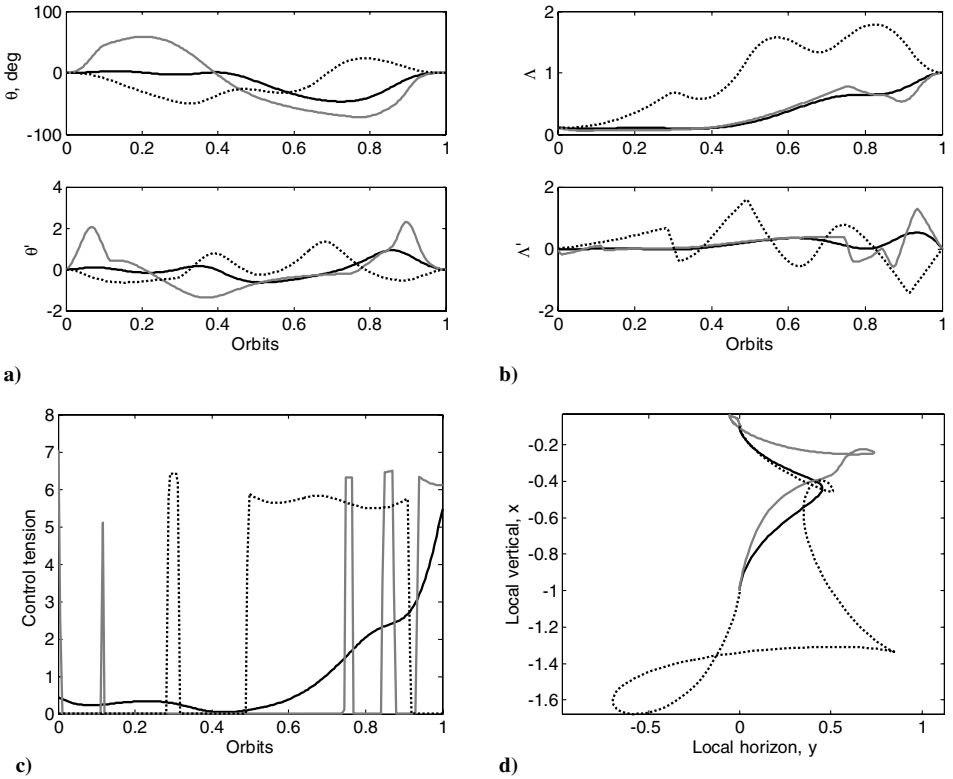

Fig. 2 Optimal deployment trajectories for the rigid tether, where the black solid line represents the minimum tension, the gray solid line represents the minimum l_1 tension, and the dashed line represents the maximum tension: a) libration dynamics, b) length dynamics, c) control tension, and d) deployment path in orbital frame.

Figure 3 shows optimal deployment trajectories for the minimum tension rate, minimum power, and minimum angle cost functions. Again, there are some similarities between the minimum power and minimum tension rate trajectories, but the minimum tension rate is clearly the best of this group. One of the features of the minimum power trajectory is that the tension tends to peak in regions where the length rate is low. This makes sense because the cost function is essentially the projection of the tension force with the deployment rate. Hence, the contribution of the tension to the cost is negligible when the length rate is small or zero. The tension peaks cause significant peaks in the reel acceleration. For example, in nondimensional units, the maximum reel acceleration is 0.325 for the minimum tension rate, whereas it peaks at 3.36 and 6.51 for the minimum power and minimum angle trajectories, respectively. The behavior of the minimum power trajectory should be contrasted with the minimum tension rate trajectory, which shows an extremely smooth tension profile and correspondingly smooth length and length rate variations. An examination of the minimum angle trajectory illustrates that, although the angle is kept "small" in an integral sense (maximum angle is 27.9 deg), the variation in the angle and motion of the subsatellite in the orbital frame is quite considerable. For example, the maximum libration rate is quite large compared with the other trajectories (compare 1.13 with 0.56 and 0.63 for the minimum tension rate and power, respectively). Comparing the maximum deviation of the subsatellite along the local horizontal for the minimum angle trajectory with the deviations for the minimum tension rate and power illustrates the point. The control tension for the minimum angle is of a bang–bang nature with 9 switches, which results in extremely large reel accelerations of 6.51 in nondimensional units. The reel-rate requirement is almost four times the requirements for the other two trajectories. Thus, within this group, the minimum tension rate appears to be a very good choice for the performance index.

Figure 4 shows the optimal deployment trajectories for the minimum angle rate, minimum angle acceleration, and minimum length rate cost functions. The minimum libration rate trajectory demonstrates a nearly linear variation in the libration rate over the majority of the trajectory, resulting in a relatively low peak libration angle (23.8 deg). In fact, the maximum libration angle is almost 4 deg better than the minimum libration angle trajectory. The minimum libration acceleration trajectory shows a smooth variation in the libration rate with the lowest recorded libration rate of the results presented thus far (in fact, it is second only to the minimax libration rate trajectory overall). All of the trajectories shown in Fig. 4 have relatively large reel acceleration requirements just before the final time (3.36 in nondimensional units). The minimum reel-rate trajectory has a peak reel rate of 25.85 m/s, whereas the minimum libration acceleration only requires an additional 0.48 m/s. Thus, the minimum libration acceleration appears to be superior within this group of performance indices. However, all of the trajectories have significant spikes in the tether tension at the final time, making these trajectories undesirable.

Figure 5 shows the optimal deployment trajectories for the minimum reel acceleration, minimum tension acceleration, and minimum time cost functions. The minimum time for the deployment is approximately 0.529 of one orbit, or 50.05 min in dimensional time. However, the fast deployment time requires relatively large libration angles (54.6 deg) and high deployment rates (142.7 m/s). The control tension is of a bang–bang nature with 3 switches. The minimum time trajectory does not require the tether to be deployed only, but has a period in which the tether must be retrieved. The minimum reel and tension acceleration trajectories both have low peaks in the libration angle, but the minimum reel acceleration trajectory has the smoothest variations in length rate and libration rate. The minimum tension acceleration trajectory has a nearly uniform variation in the tether tension. The trajectory keeps quite close to the local vertical, which contrasts with the minimum time trajectory, which has significant deviations in the local horizontal direction.

Figure 6 shows the optimal deployment trajectories for the minimax angle, minimax angle rate, and minimax angle acceleration cost functions. In the minimax angle trajectory, the tether is deployed at nearly a constant angle (17.71 deg). However, the control tension

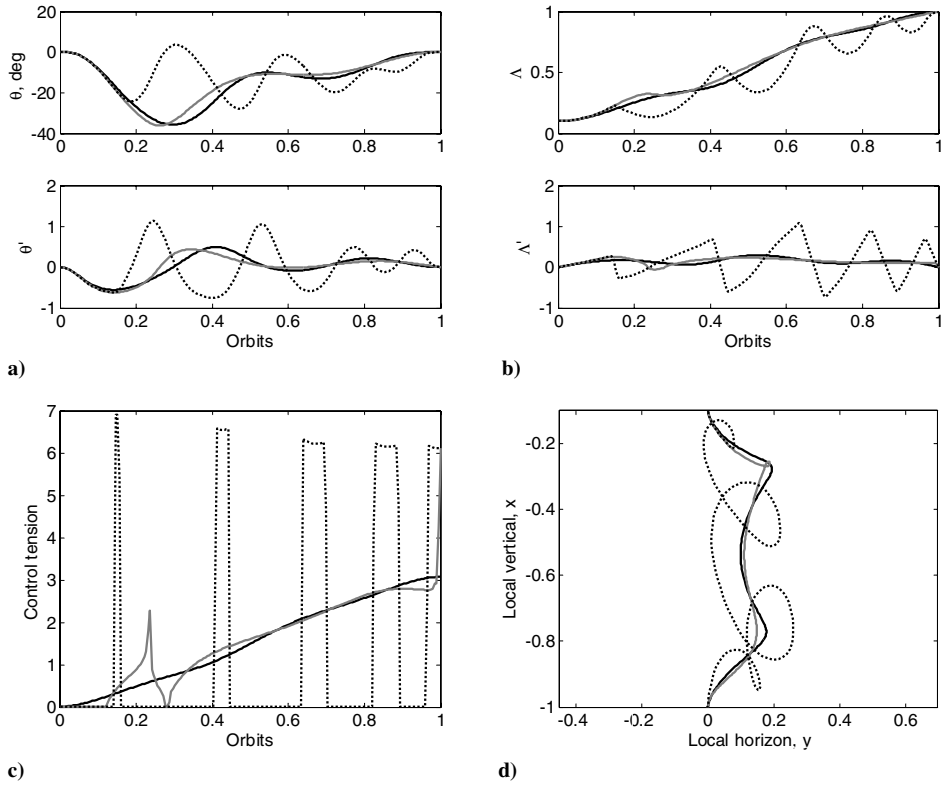

Fig. 3 Optimal deployment trajectories for the rigid tether, where the black solid line represents the minimum tension rate, the gray solid line represents the minimum power, and the dashed line represents the minimum angle: a) libration dynamics, b) length dynamics, c) control tension, and d) deployment path in orbital frame.

chatters along this boundary. It is interesting to note that the horizontal deviation of the subsatellite is approximately the same for the minimax angle and the minimax angle acceleration trajectories. It can be seen that the lowest horizontal deviation is actually produced by the minimax angle rate trajectory. The minimax angle acceleration trajectory shows segments with nearly linear variations of angular rate, demonstrating the bang–bang nature of the angle acceleration. None of these trajectories would be suitable for

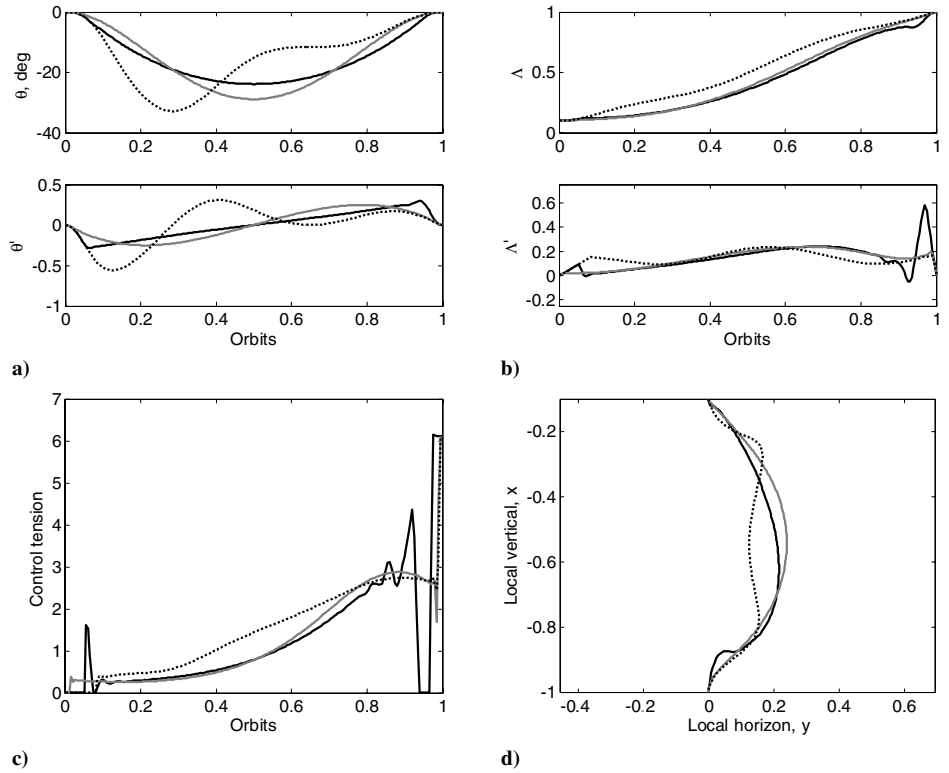

Fig. 4 Optimal deployment trajectories for the rigid tether, where the black solid line represents the minimum angle rate, the gray solid line represents the minimum angle acceleration, and the dashed line represents the minimum length rate: a) libration dynamics, b) length dynamics, c) control tension, and d) deployment path in orbital frame.

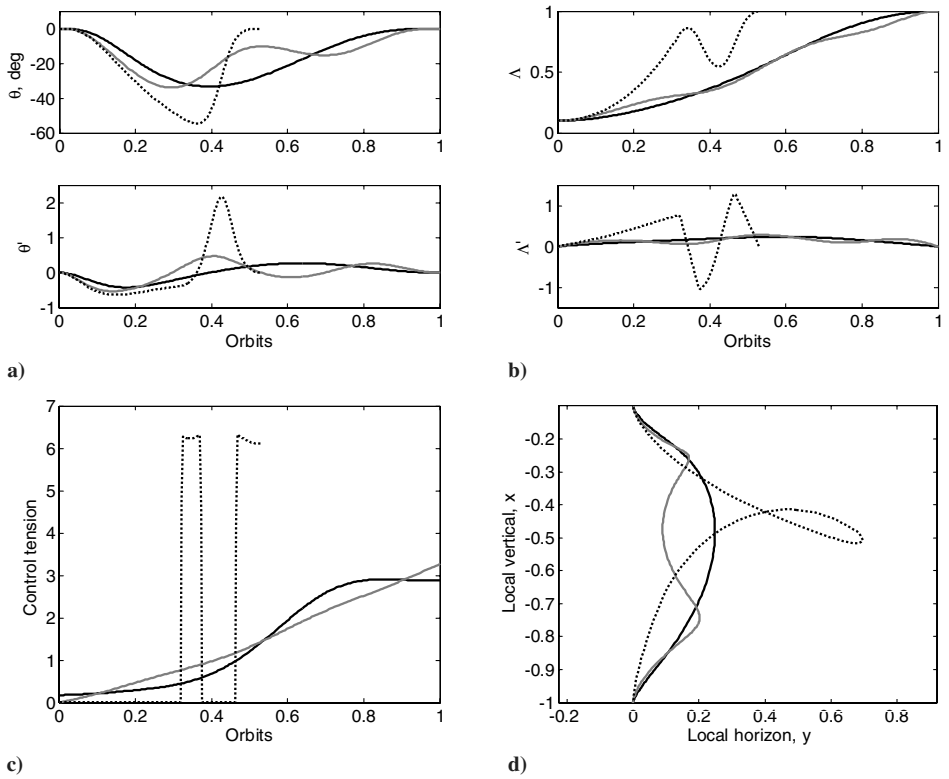

Fig. 5 Optimal deployment trajectories for the rigid tether, where the black solid line represents the minimum length acceleration, the gray solid line represents the minimum tension acceleration, and the dashed line represents the minimum time: a) libration dynamics, b) length dynamics, c) control tension, and d) deployment path in orbital frame.

implementation because of the significant spikes in the control tensions. In addition, the minimax angle requires very high maximum length accelerations and a maximum reel rate on the order of 96 m/s.

Figure 7 shows the optimal deployment trajectories for the minimax length rate, minimax length acceleration, and minimax tension cost functions. The minimax tension trajectory is of a bang–bang nature with 3 switches, which causes relatively large libration

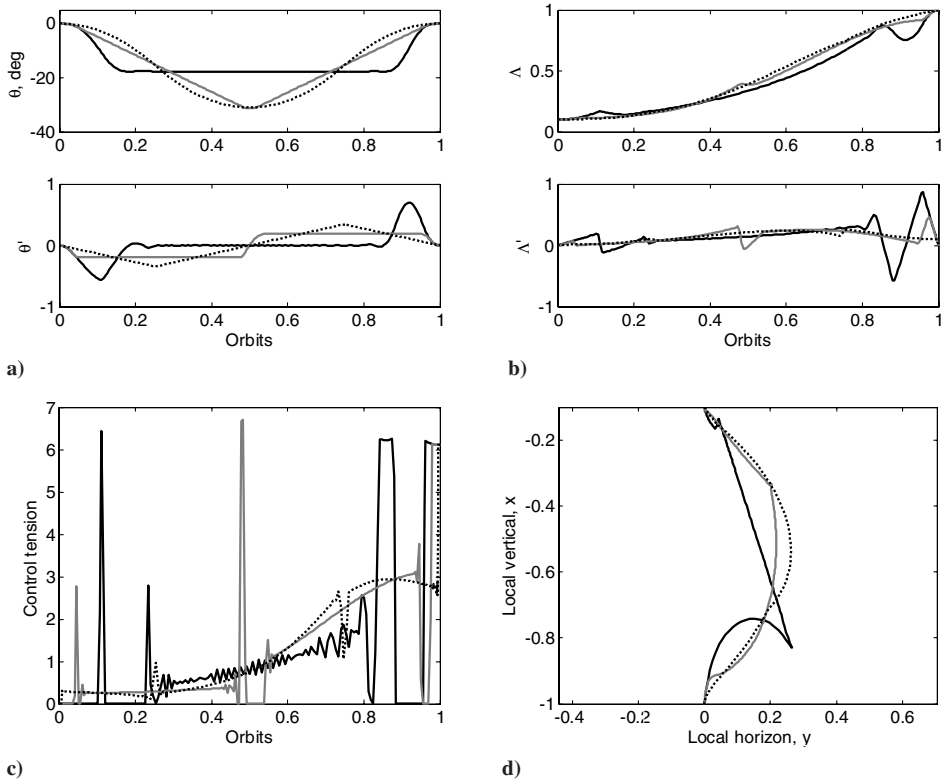

Fig. 6 Optimal deployment trajectories for the rigid tether, where the black solid line represents the minimax angle, the gray solid line represents the minimax angle rate, and the dashed line represents the minimax angle acceleration: a) libration dynamics, b) length dynamics, c) control tension, and d) deployment path in orbital frame.

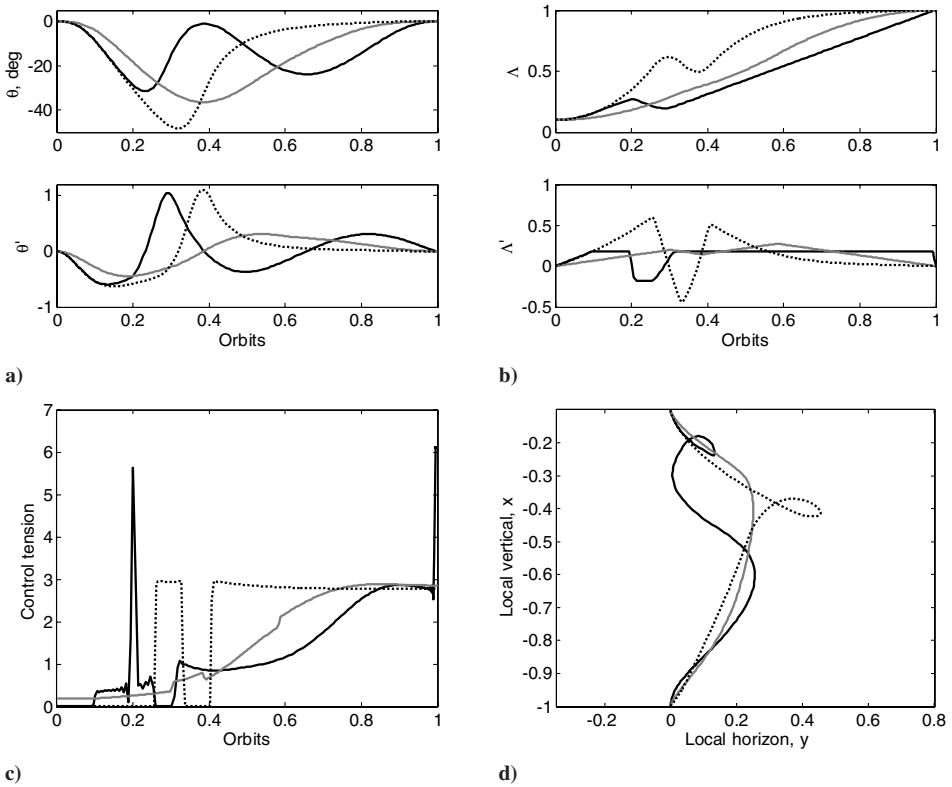

Fig. 7 Optimal deployment trajectories for the rigid tether, where the black solid line represents the minimax length rate, the gray solid line represents the minimax length acceleration, and the dashed line represents the minimax tension: a) libration dynamics, b) length dynamics, c) control tension, and d) deployment path in orbital frame.

angles (48.3 deg) and reel rates (66.3 m/s). The minimax reel-rate trajectory shows the best achievable reel rate for the given scenario, which is 20.3 m/s. However, the trajectory shows quite large peaks in the control tension, corresponding to high nondimensional length accelerations (5.213). The minimax length acceleration trajectory shows that the best achievable length acceleration for this deployment scenario is 0.1051 in nondimensional units. This compares well with the maximum length acceleration experienced for the minimum length acceleration cost function (0.1265). Notice how much better these trajectories are compared with most of the other trajectories presented thus far. The maximum reel rate required in this case is approximately 30.2 m/s.

Figure 8 shows the optimal deployment trajectories for the minimax tension rate and tension acceleration cost functions. These trajectories are very close to each other in every sense, even in terms of the sensitive control tension. It is evident that the tension varies in a nearly linear fashion for both cases. The minimax tension acceleration has a smoother variation in tension than the minimax tension rate and would thus be the preferable of the two.

By invoking the symmetry of deployment/retrieval theorem, we know that the optimal retrieval trajectories generate the same cost as the deployment trajectories, as well as the same dynamics satisfying certain relationships stated in Sec. III.D. Hence, there is no need to compute the retrieval trajectories. For numerical confirmation, additional computations were performed that produced results consistent with the theorem, indicating the successful convergence of the numerical optimization algorithm used in this work.

A summary of the maximum absolute values of the states and accelerations observed in the optimal trajectories are listed in Table 4 for each of the cost functions. An examination of Table 4 clearly demonstrates that the minimum value of each state variable is achieved in the minimax cost functions. One possible way of comparing these results is to calculate the norm of the maximum state values and accelerations for each cost. This gives an indication of the overall variation of the states and control. Note, the maximum angle should be first expressed in radians. After performing the calculations for the l_2 norm and ranking the costs, it is apparent that the minimum length acceleration is the best cost function (1.40) [value of norm in parenthesis]. This is followed closely by the minimax length acceleration trajectory (1.45). These are followed by the minimum tension acceleration (1.73), minimum tension rate (1.74), minimax tension acceleration (1.75), and minimax tension rate trajectories (1.83). The maximum norms of the next best cost functions (minimax angle acceleration, 3.58) are approximately double the minimax tension rate trajectory, which indicates that the best-performing trajectories are significantly better than the remaining trajectories. The worst performer is the minimum l_1 tension (10.72), followed by the minimum time trajectory (9.73). Thus, it is apparent that a cost function that penalizes the tether length acceleration produces the least deviation in the state variables. Furthermore, minimizing the rate or acceleration of the tether tension may also be considered a good measure in terms of the deviations of the states during the trajectory. Note that the order of results is only slightly altered if the costs are ranked in terms of the l_1 norm.

2. *Sensitivity Analysis*

The trajectories generated in the previous section are representative of the results that can be expected for different system parameters. In other words, the choice of a "poor" cost function will always give undesirable results regardless of the system parameters and boundary conditions. In this section, the effects of different system parameters on the best-performing trajectories is considered. Variations in total tether length, substatellite mass, orbit altitude, tether density, mother satellite mass, initial length, and initial angle are considered. Table 5 summarizes the ranges of the variables and the resulting percentage change in the maximum state variables.

The results show that the trajectories are least sensitive to orbit altitude. This is due to the nondimensional nature of the trajectories. The orbit altitude affects the orbital angular velocity, which impacts the trajectories only through the tension constraint. Hence, the trajectories remain unaltered unless the nominal trajectory is

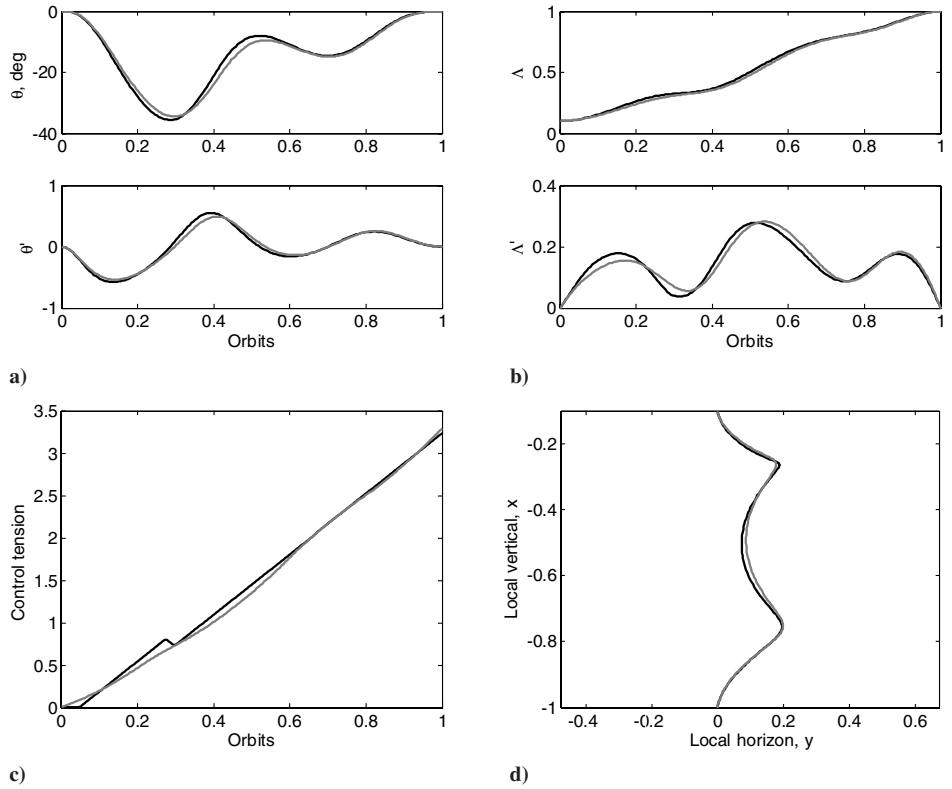

Fig. 8 Optimal deployment trajectories for the rigid tether, where the black solid line represents the minimax tension rate, the gray solid line represents the minimax tension acceleration: a) libration dynamics, b) length dynamics, c) control tension, and d) deployment path in orbital frame.

saturated on the tension constraint. Note that, to compensate for large changes in tension due to changes in the system parameters, the upper tension constraint is scaled according to $T_{\max} = T^0_{\max}(m_s/500)(L_f/100,000)$. The next least-sensitive parameters are the tether length and end mass values. For example, the maximum change in the libration angle is 1.73% for an increase in tether length of 200 km for the minimum reel acceleration trajectory. The maximum change in the libration angle of 6% occurs for the minimax length acceleration trajectory due to an increase in tether density by 9 kg/km. The impact of tether density is on the tether mass, which is not directly taken into consideration in the scaling of the maximum tension constraint. As can be expected, changes to the initial conditions alter the trajectories most significantly relative to the nominal trajectories. For example, the librational acceleration for the minimum reel acceleration case is double that of the nominal case for an initial libration angle of 20 deg. However, the change in maximum reel acceleration for the same case is only 7.81%. This indicates that only moderate changes in the control are required for changes in the initial conditions. The effects of different initial conditions on the libration angle and length rate are shown in Fig. 9. These results clearly illustrate that the essential nature of the optimal reel rate remains unaltered with relatively large changes to the initial conditions. That is, the selection of a "good" cost function will always give well-behaved system dynamics.

Table 4 Maximum states and accelerations for optimal deployment/retrieval with inelastic tether

Cost	Max $\lvert\theta\rvert$, deg	Max $\lvert\theta'\rvert$	Max $\lvert\theta''\rvert$	Max $\lvert\Lambda\rvert$	Max $\lvert\Lambda'\rvert$	Max $\lvert\Lambda''\rvert$
$\mathcal{J}_1^r$ min. tension	46.75	0.940	1.669	1	0.524	2.735
$\mathcal{J}_2^r$ min. l_1 tension	72.22	2.301	7.729	1	1.293	6.760
$\mathcal{J}_3^r$ max. tension	49.95	1.346	2.695	1.7843	1.580	5.963
$\mathcal{J}_4^r$ max. l_1 tension	49.95	1.346	2.695	1.7843	1.580	5.963
$\mathcal{J}_5^r$ min. tension rate	35.74	0.557	1.075	1	0.290	0.325
$\mathcal{J}_6^r$ min. power	36.19	0.625	1.770	1	0.254	3.359
$\mathcal{J}_7^r$ min. angle	27.89	1.131	4.121	1	1.083	6.505
$\mathcal{J}_8^r$ min. angle rate	23.85	0.297	1.407	1	0.581	3.359
$\mathcal{J}_9^r$ min. angle accel.	28.87	0.251	0.416	1	0.238	3.359
$\mathcal{J}_{10}^r$ min. length rate	32.81	0.559	1.155	1	0.234	3.359
$\mathcal{J}_{11}^r$ min. length accel.	33.31	0.420	0.619	1	0.238	0.127
$\mathcal{J}_{12}^r$ min. tension accel.	33.89	0.530	1.005	1	0.282	0.519
$\mathcal{J}_{13}^r$ min. time	54.65	2.158	7.189	1	1.289	5.900
$\mathcal{J}_{14}^r$ minimax angle	17.71	0.696	2.751	1	0.869	6.100
$\mathcal{J}_{15}^r$ minimax angle rate	31.31	0.189	1.598	1	0.465	5.988
$\mathcal{J}_{16}^r$ minimax angle accel.	30.94	0.341	0.221	1	0.259	3.359
$\mathcal{J}_{17}^r$ minimax length rate	31.52	1.047	3.371	1	0.184	5.213
$\mathcal{J}_{18}^r$ minimax length accel.	36.51	0.446	0.653	1	0.273	0.105
$\mathcal{J}_{19}^r$ minimax tension	48.30	1.102	3.613	1	0.599	2.704
$\mathcal{J}_{20}^r$ minimax tension rate	35.62	0.574	1.152	1	0.278	0.487
$\mathcal{J}_{21}^r$ minimax tension accel.	34.48	0.536	1.015	1	0.282	0.545

Table 5 Percentage change in maximum absolute values of state variables because of parameter variations for rigid tether

	Minimum tension rate					Minimum reel acceleration					Minimum tension acceleration					Minimax length acceleration				
	$\Delta\theta_{max}$	$\Delta\theta'_{max}$	$\Delta\theta''_{max}$	$\Delta\Lambda'_{max}$	$\Delta\Lambda''_{max}$	$\Delta\theta_{max}$	$\Delta\theta'_{max}$	$\Delta\theta''_{max}$	$\Delta\Lambda'_{max}$	$\Delta\Lambda''_{max}$	$\Delta\theta_{max}$	$\Delta\theta'_{max}$	$\Delta\theta''_{max}$	$\Delta\Lambda'_{max}$	$\Delta\Lambda''_{max}$	$\Delta\theta_{max}$	$\Delta\theta'_{max}$	$\Delta\theta''_{max}$	$\Delta\Lambda'_{max}$	$\Delta\Lambda''_{max}$
Tether length																				
20 km	0.07	0.04	−0.36	0.45	1.01	−0.79	−0.56	−0.52	0.42	0.27	−0.48	−0.88	−2.13	0.18	3.67	−0.73	−0.16	0.30	0.36	0.08
50 km	0.10	0.21	0.48	0.23	0.46	−0.48	−0.34	−0.33	0.26	0.36	−0.06	−0.16	−0.43	0.09	2.29	−0.45	−0.10	0.74	0.22	0.04
150 km	−0.06	−0.15	−0.36	−0.23	−0.56	0.47	0.34	0.35	−0.25	−0.15	−0.06	−0.03	0.02	−0.11	−2.09	0.46	0.10	0.33	−0.22	−0.03
200 km	−0.08	−0.27	−0.64	−0.46	−1.20	0.91	0.66	0.66	−0.49	−0.17	−0.16	−0.11	−0.07	−0.24	−3.99	0.88	0.21	−0.40	−0.43	−0.04
250 km	−0.08	−0.35	−0.85	−0.67	−1.86	1.33	0.96	1.00	−0.73	−0.11	−0.27	−0.22	−0.21	−0.39	−5.70	1.29	0.32	−0.18	−0.62	−0.04
300 km	−0.05	−0.41	−1.01	−0.87	−2.52	1.73	1.25	1.29	−0.96	−0.14	−0.40	−0.35	−0.38	−0.55	−7.27	1.68	0.44	−0.78	−0.81	−0.03
Subsatellite mass																				
100 kg	1.16	−0.11	−1.52	−1.37	−4.88	4.23	3.02	3.19	−2.38	0.21	−0.30	−1.31	−3.04	−0.92	−14.07	4.16	1.12	−1.77	−2.09	0.03
200 kg	0.31	−0.10	−0.55	−0.53	−1.88	1.73	1.21	1.20	−0.95	−0.30	−0.08	−0.43	−1.09	−0.19	−6.42	1.66	0.40	−0.86	−0.82	−0.08
300 kg	0.10	−0.09	−0.34	−0.25	−0.78	0.80	0.56	0.54	−0.43	−0.26	−0.03	−0.18	−0.47	−0.05	−3.06	0.76	0.17	−0.52	−0.37	−0.05
400 kg	0.03	−0.04	−0.15	−0.09	−0.28	0.31	0.23	0.24	−0.16	−0.16	−0.01	−0.06	−0.18	−0.01	−1.20	0.29	0.06	−0.05	−0.14	−0.02
600 kg	−0.01	0.04	0.12	0.06	0.17	−0.21	−0.16	−0.15	0.11	0.19	0.00	0.04	0.11	−0.00	0.82	−0.19	−0.04	0.48	0.09	0.02
700 kg	−0.02	0.07	0.21	0.11	0.28	−0.33	−0.22	−0.21	0.19	−0.01	0.00	0.07	0.19	−0.00	1.43	−0.32	−0.07	0.81	0.16	0.03
800 kg	−0.02	0.09	0.28	0.14	0.36	−0.44	−0.30	−0.30	0.25	0.05	0.00	0.09	0.25	−0.00	1.89	−0.42	−0.09	0.76	0.21	0.04
900 kg	−0.02	0.11	0.34	0.17	0.42	−0.53	−0.36	−0.34	0.29	0.08	0.01	0.10	0.30	−0.00	2.26	−0.50	−0.11	0.70	0.25	0.05
1000 kg	−0.02	0.13	0.39	0.19	0.47	−0.60	−0.40	−0.36	0.33	0.09	0.01	0.11	0.34	−0.00	2.55	−0.57	−0.12	0.67	0.28	0.06
Altitude																				
300 km	0	0	0	0	0	0	0	0	0	0	0.01	0.02	0.05	−0.00	0.01	0	0	0	0	0
400 km	0	0	0	0	0	0	0	0	0	0	0.01	0.01	0.02	−0.00	0.00	0	0	0	0	0
600 km	0	0	0	0	0	0	0	0	0	0	−0.01	−0.01	−0.02	0.00	−0.00	0	0	0	0	0
700 km	0	0	0	0	0	0	0	0	0	0	−0.01	−0.02	−0.05	0.00	−0.01	0	0	0	0	0
800 km	0	0	0	0	0	0	0	0	0	0	−0.02	−0.03	−0.08	0.00	−0.01	0	0	0	0	0
900 km	0	0	0	0	0	0	0	0	0	0	−0.03	−0.05	−0.11	0.00	−0.02	0	0	0	0	0
1000 km	0	0	0	0	0	0	0	0	0	0	−0.04	−0.06	−0.14	0.00	−0.02	0	0	0	0	0
Tether density																				
2 kg/km	−0.08	−0.27	−0.63	−0.46	−1.20	0.91	0.67	0.71	−0.49	−0.10	−0.25	−0.25	−0.37	−0.24	−4.04	0.88	0.21	−0.40	−0.43	−0.04
3 kg/km	−0.05	−0.41	−1.01	−0.88	−2.53	1.72	1.23	1.27	−0.96	−0.03	−0.52	−0.53	−0.77	−0.56	−7.36	1.68	0.44	−0.78	−0.81	−0.03
4 kg/km	0.05	−0.47	−1.22	−1.29	−3.83	2.47	1.80	1.90	−1.38	0.01	−0.81	−0.84	−1.21	−0.93	−10.10	2.44	0.67	−1.16	−1.16	0.02
5 kg/km	0.21	−0.49	−1.33	−1.71	−5.07	3.15	2.31	2.50	−1.78	0.22	−1.12	−1.18	−1.65	−1.33	−12.41	3.14	0.91	−1.21	−1.49	0.09
6 kg/km	0.38	−0.48	−1.37	−2.12	−6.22	3.76	2.80	3.10	−2.14	0.59	−1.42	−1.51	−2.10	−1.74	−14.37	3.80	1.15	−0.86	−1.77	0.20
7 kg/km	0.55	−0.45	−1.38	−2.53	−7.28	4.31	3.24	3.67	−2.47	0.93	−1.73	−1.86	−2.56	−2.16	−16.04	4.41	1.40	−1.27	−2.03	0.32
8 kg/km	0.73	−0.41	−1.36	−2.90	−8.25	4.83	3.67	4.22	−2.77	1.30	−2.04	−2.21	−3.01	−2.58	−17.48	4.97	1.65	−1.08	−2.25	0.46
9 kg/km	0.88	−0.40	−1.42	−3.27	−9.14	5.29	4.04	4.73	−3.04	1.66	−2.37	−2.56	−3.46	−2.99	−18.70	5.51	1.89	−1.13	−2.45	0.61
10 kg/km	1.00	−0.44	−1.59	−3.64	−9.94	5.71	4.40	5.25	−3.29	2.10	−2.68	−2.91	−3.91	−3.39	−19.76	6.00	2.14	−0.60	−2.61	0.77
Mother satellite mass																				
2500 kg	−0.24	−0.15	−0.16	−0.09	−0.00	−0.27	−0.18	−0.15	0.14	0.11	−0.38	−0.23	−0.24	−0.16	0.31	−0.24	−0.05	0.63	0.12	0.03
7500 kg	0.08	0.05	0.06	0.03	−0.00	0.09	0.07	0.08	−0.04	−0.04	0.12	0.08	0.08	0.05	−0.12	0.08	0.02	0.05	−0.04	−0.01
10,000 kg	0.13	0.08	0.09	0.04	−0.01	0.13	0.11	0.14	−0.07	−0.08	0.19	0.11	0.12	0.07	−0.18	0.13	0.02	0.08	−0.06	−0.02
25,000 kg	0.20	0.13	0.14	0.07	−0.02	0.22	0.17	0.18	−0.11	−0.01	0.30	0.18	0.19	0.12	−0.29	0.20	0.04	0.12	−0.10	−0.03
50,000 kg	0.23	0.14	0.16	0.08	−0.02	0.24	0.19	0.23	−0.12	−0.10	0.34	0.21	0.21	0.13	−0.32	0.23	0.04	0.15	−0.11	−0.03

(continued)

Table 5 Percentage change in maximum absolute values of state variables because of parameter variations for rigid tether (Continued)

	Minimum tension rate					Minimum reel acceleration					Minimum tension acceleration					Minimax length acceleration				
	$\Delta\theta_{\max}$	$\Delta\theta'_{\max}$	$\Delta\theta''_{\max}$	$\Delta\Lambda'_{\max}$	$\Delta\Lambda''_{\max}$	$\Delta\theta_{\max}$	$\Delta\theta'_{\max}$	$\Delta\theta''_{\max}$	$\Delta\Lambda'_{\max}$	$\Delta\Lambda''_{\max}$	$\Delta\theta_{\max}$	$\Delta\theta'_{\max}$	$\Delta\theta''_{\max}$	$\Delta\Lambda'_{\max}$	$\Delta\Lambda''_{\max}$	$\Delta\theta_{\max}$	$\Delta\theta'_{\max}$	$\Delta\theta''_{\max}$	$\Delta\Lambda'_{\max}$	$\Delta\Lambda''_{\max}$
Initial length																				
5 km	25.66	12.61	6.94	10.80	23.88	31.03	36.41	75.42	4.92	25.95	18.71	12.86	13.11	8.95	21.17	32.67	33.13	60.83	7.19	16.90
6 km	19.53	11.30	7.13	9.00	17.27	22.91	26.55	51.04	3.81	17.61	15.25	10.43	10.59	7.42	13.59	24.13	24.75	41.06	5.50	12.10
7 km	14.01	9.14	7.24	6.67	11.78	16.03	18.37	33.35	2.79	11.19	10.80	7.22	7.00	5.53	8.77	16.86	17.41	26.03	3.98	8.30
8 km	8.97	6.42	6.63	4.32	7.15	10.04	11.43	19.70	1.83	6.56	6.78	4.45	4.15	3.65	5.16	10.56	10.97	14.09	2.58	5.14
9 km	4.35	3.36	4.27	2.06	3.19	4.75	5.39	8.90	0.91	2.88	3.18	2.06	1.87	1.80	2.31	4.99	5.21	4.24	1.27	2.41
Initial angle																				
−20 deg	−2.41	−12.95	−10.71	−1.84	−2.34	−4.10	−16.80	−13.30	−1.02	2.32	−2.07	−13.43	−10.91	−1.67	−4.31	−3.49	−14.42	−3.58	−0.84	−0.48
−15 deg	−4.50	−19.96	−19.49	−3.53	−4.48	−7.86	−31.06	−17.15	−2.03	4.65	−3.82	−19.47	−20.08	−3.19	−8.42	−6.75	−25.86	−6.56	−1.68	−0.80
−10 deg	−6.19	−23.83	−26.07	−5.04	−6.39	−11.31	−40.43	21.12	−3.01	6.78	−5.20	−23.51	−25.38	−4.57	−12.29	−9.74	−34.73	14.80	−2.53	−1.01
−5 deg	−7.41	−27.26	−10.32	−6.37	−8.06	−14.49	−42.03	55.71	−3.96	8.39	−6.15	−27.25	−4.07	−5.79	−15.90	−12.51	−36.37	47.58	−3.39	−1.16
5 deg	2.65	13.26	12.12	1.99	5.46	4.46	19.16	19.94	1.03	−0.00	2.35	13.80	12.40	1.80	4.50	3.70	17.16	13.99	0.82	0.67
10 deg	5.48	26.47	24.21	4.17	12.51	9.26	40.16	45.20	2.05	1.66	5.01	27.93	25.68	3.68	9.10	7.52	36.35	37.98	1.61	1.55
15 deg	8.52	39.82	36.44	6.44	19.72	14.39	62.26	72.91	3.06	4.50	7.93	42.24	38.89	5.67	13.87	11.37	56.82	65.28	2.38	2.67
20 deg	11.72	53.09	47.67	8.81	26.82	19.79	85.00	100.90	4.05	7.81	11.08	56.70	51.68	7.70	18.75	15.14	77.66	92.73	3.13	4.01

B. Flexible Tether Trajectories

1. Nominal Trajectories

In this section, a summary of some of the trajectories for an elastic tether are presented rather than all of the solutions. Optimal deployment trajectories are shown in Fig. 10 for the minimum tension, maximum tension, and minimum strain rate cost functions. In the case of an elastic tether, the optimal trajectories are quite different than those of an inelastic tether. The main reason for the difference is not due to fundamental differences in the dynamics of the two systems. That is, the rigid body dynamics are almost unaffected by the longitudinal vibrations. Rather, the optimal control problem must deal with the control of the tether strain variables in addition to the tether length and librational dynamics, that is, the tether strain must satisfy certain boundary conditions. This is a central concept being explored in this paper. Simply posing an optimal control problem with desired boundary conditions does *not* ensure a well-behaved trajectory. This is exemplified by examining the tether strain time history. The effect of the longitudinal vibrations on the reel acceleration is also apparent. The effect is most significant for the maximum tension trajectory. In the case of a rigid tether, the tension must be controlled to be large by only changing the tether length. In the case of an elastic tether, the tension can be made large by both changing the tether length and initiating longitudinal vibrations. For these three trajectories, it is evident that the minimum strain rate cost function generates relatively smooth trajectories. It reaches a maximum libration angle of 31.12 deg and requires a maximum reel rate of approximately 30.10 m/s. This should be compared with the reel requirements for the minimum tension (46.15 m/s) and maximum tension (96.07 m/s) trajectories.

Figure 11 shows the optimal deployment trajectories for the minimum length acceleration, minimum unstrained length acceleration, and minimum strain acceleration cost functions. The minimum total length acceleration trajectory produces very smooth variations in strain, whereas the minimum unstrained length acceleration results in longitudinal oscillations of the tether. The results also show that there is a strong similarity between the total and unstrained length acceleration trajectories. This is due to the relatively weak coupling between strain variations and librations. Similar behavior is observed for the minimum length rate and unstrained length rate cost functions (not shown). An important point to note is that the trajectories are almost identical to the rigid minimum length acceleration trajectories. This illustrates that not only is the minimum length acceleration cost function an excellent choice for a rigid tether, but that it is also an excellent choice for an elastic tether. Thus, by properly selecting the cost function, desired features in the dynamics can be achieved in both the elastic and inelastic models. Finally, the minimum strain acceleration trajectory exhibits a reasonably well-behaved set of dynamics. One of the main differences between it and the minimum length acceleration trajectories is that the tether is deployed more slowly initially and has a large increase in the length rate near the end of deployment. The length rate drops off relatively quickly, leading to larger reel accelerations at the terminal stages of deployment.

Figure 12 shows the cost functions belonging to the minimax strain rate and minimax strain acceleration trajectories. These trajectories are noticeably different from each other, but nevertheless are two of the best-performing trajectories for an elastic tether in terms of the longitudinal dynamics. However, the minimax strain acceleration trajectory is without question the best of the elastic tether trajectories. It has some excellent features such as a peak libration angle of about 30.3 deg, comparatively small libration rates and accelerations, a peak reel rate of approximately 28.4 m/s, and relatively small maximum reel accelerations (0.37). The most important feature is the extremely smooth variation in the tether strain. It is evident that the optimal solution contains a bang–bang variation in the strain acceleration, which gives a linear variation in strain rate and quadratic variations in the strain. It is important to point out that the tether strain stays well above the lower limit and well below the upper limit throughout the trajectory. Hence, this appears to be the best-candidate cost function for an elastic tether.

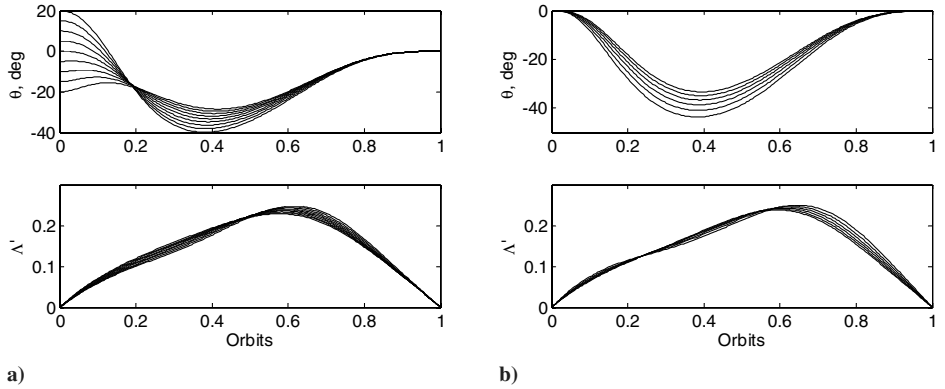

Fig. 9 Effect of different initial conditions on the minimum reel acceleration angle and length rate: a) initial angle, and b) initial length.

Table 6 summarizes the maximum states and accelerations for optimal deployment/retrieval with an elastic tether. Clearly, the symmetry of the deployment/retrieval phases allows us to circumvent recalculating the retrieval trajectories. The minimum angle trajectory has a maximum libration angle of 27.4 deg, which is approximately 10 deg larger than the minimax libration angle. The main feature of the dynamics is that the angle oscillates back and forth from approximately 0 to 27 deg, incurring large libration rates and accelerations. In a similar manner to the rigid tether trajectories, the strain saturates on several occasions, behaving in a bang–bang-like manner. This induces quite large nondimensional strain rates (0.208) and accelerations (122.9). As a consequence, high reel accelerations (15.89) are necessary to control the longitudinal dynamics. The minimum power trajectory resembles the rigid tether trajectory quite well, including the strain/tension variation. The required reel rate is quite reasonable (27.9 m/s), but the longitudinal vibrations may be troublesome for a real system (maximum strain acceleration is 9.23). Like the previous results for a rigid tether, the minimum angle rate produces a smaller maximum libration angle than the minimum angle cost function (23.9 deg). The minimum angle rate trajectory is better in every regard than the minimum angle trajectory, but the strain acceleration is unacceptably large (22.3). The strain acceleration for the minimum angle acceleration (22.4), minimum length rate (20.8), and minimum unstrained length rate (23.2) are likewise very large, resulting in large reel accelerations. None of these trajectories would be suitable for implementation in a practical system.

The minimum time trajectories are very similar to the minimum time trajectories for a rigid tether and demonstrate a bang–bang variation in strain. In the case of an elastic tether, however, extremely large reel accelerations are required to produce this variation. The strain accelerations are extremely large for the minimum time (302.9), minimax angle (330.1), and minimax angle rate (402.5), with correspondingly large reel accelerations (minimum time is 48.2; minimax angle is 85.7; minimax angle rate is 40.2). As observed for the rigid tether case, these cost functions are not suitable for tether deployment optimization. The results for the minimax angle acceleration, minimax length rate, and minimax unstrained length rate cost functions show that the libration and unstrained length modes of the dynamics for all three cost functions are very similar to

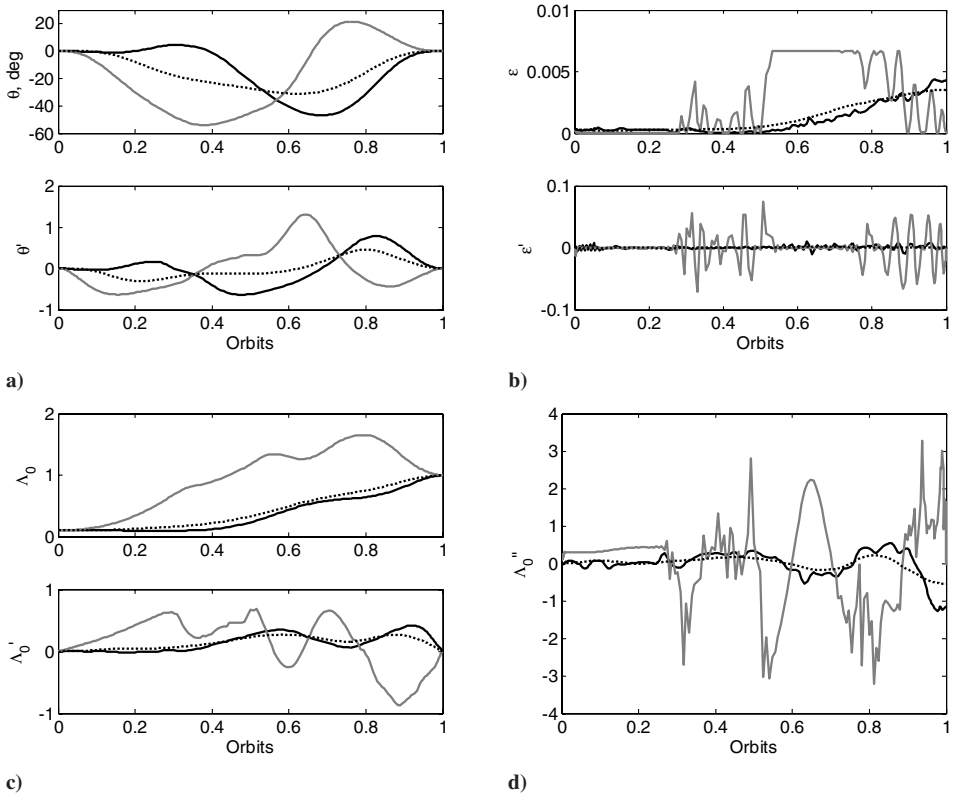

Fig. 10 Optimal deployment trajectories for the elastic tether, where the black solid line represents the minimum tension, the gray solid line represents the maximum tension, and the dashed line represents the minimum strain rate: a) libration dynamics, b) longitudinal dynamics, c) unstrained length dynamics, and d) reel acceleration.

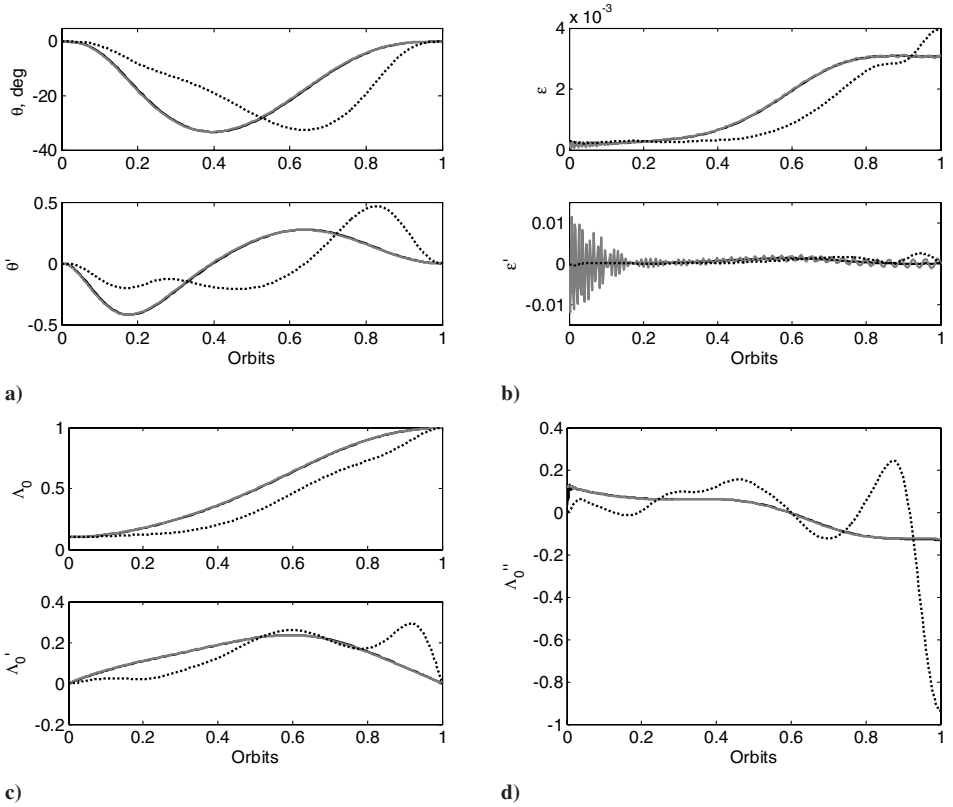

Fig. 11 Optimal deployment trajectories for the elastic tether, where the black solid line represents the minimum length acceleration, the gray solid line represents the minimum unstrained length acceleration, and the dashed line represents the minimum strain acceleration: a) libration dynamics, b) longitudinal dynamics, c) unstrained length dynamics, and d) reel acceleration.

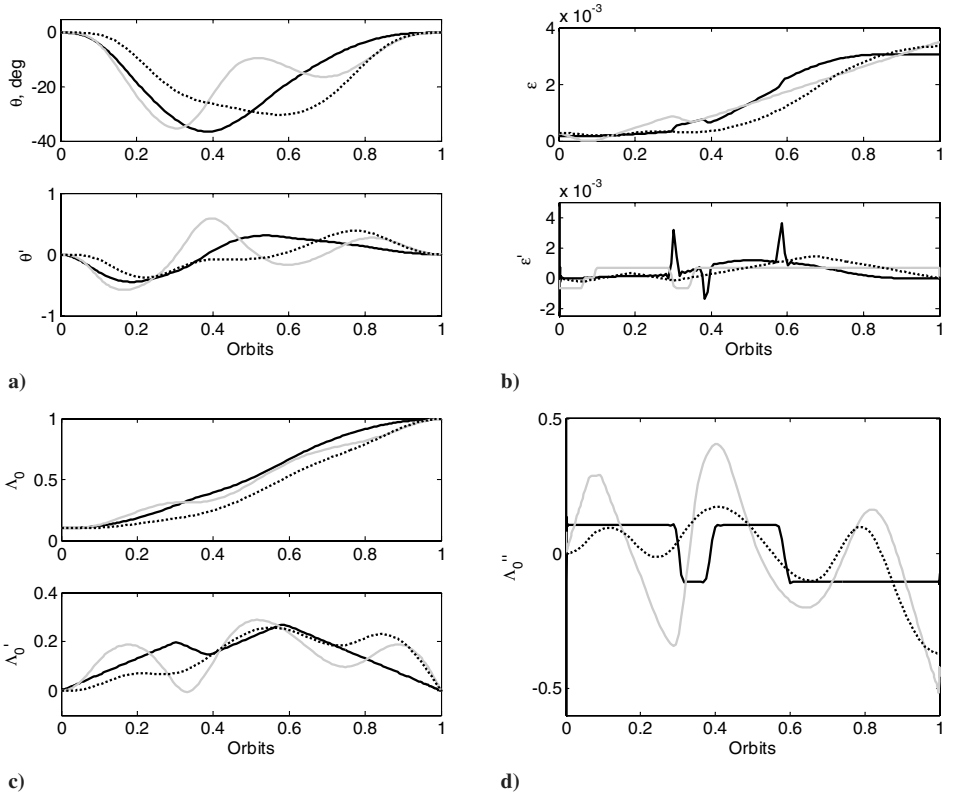

Fig. 12 Optimal deployment trajectories for the elastic tether, where the black solid line represents the minimax length acceleration, the gray solid line represents the minimax strain rate, and the dashed line represents the minimax strain acceleration: a) libration dynamics, b) longitudinal dynamics, c) unstrained length dynamics, and d) reel acceleration.

Table 6 Maximum states and accelerations for optimal deployment/retrieval with an elastic tether

Cost	Max $\|\theta\|$, deg	Max $\|\theta'\|$	Max $\|\theta''\|$	Max $\|\varepsilon\|$	Max $\|\varepsilon'\|$	Max ε''	Max $\|\Lambda_0\|$	Max $\|\Lambda_0'\|$	Max $\|\Lambda_0''\|$
$\mathcal{J}_1^e$ min. tension	47.04	0.785	1.190	4.375e − 3	1.037e − 2	0.713	0.996	0.417	1.267
$\mathcal{J}_2^e$ max. tension	54.03	1.314	2.369	6.667e − 3	7.426e − 2	3.198	1.651	0.868	3.284
$\mathcal{J}_3^e$ min. strain rate	31.12	0.456	0.580	3.520e − 3	1.517e − 3	1.201e − 2	0.996	0.272	0.542
$\mathcal{J}_4^e$ min. power	36.14	0.624	1.782	6.667e − 3	7.040e − 2	9.233	0.993	0.252	2.129
$\mathcal{J}_5^e$ min. angle	27.40	1.112	4.014	6.667e − 3	0.208	122.94	1.023	1.115	15.889
$\mathcal{J}_6^e$ min. angle rate	23.85	0.295	1.374	6.667e − 3	0.1001	22.354	0.993	0.485	3.514
$\mathcal{J}_7^e$ min. angle accel.	28.88	0.251	0.429	6.667e − 3	6.987e − 2	20.806	0.993	0.237	3.411
$\mathcal{J}_8^e$ min. length rate	32.80	0.559	1.153	6.667e − 3	8.412e − 2	23.232	0.993	0.233	4.489
$\mathcal{J}_9^e$ min. unstrained length rate	32.79	0.559	1.153	6.667e − 3	0.1044	82.923	0.993	0.232	8.299
$\mathcal{J}_{10}^e$ min. length accel.	33.34	0.418	0.613	3.084e − 3	7.266e − 3	0.829	0.997	0.237	0.130
$\mathcal{J}_{11}^e$ min. unstrained length accel.	33.32	0.420	0.630	3.111e − 3	1.203e − 2	1.272	0.997	0.237	0.127
$\mathcal{J}_{12}^e$ min. strain accel.	32.56	0.466	0.696	3.966e − 3	2.473e − 3	1.814e − 2	0.996	0.293	0.936
$\mathcal{J}_{13}^e$ min. time	54.53	2.135	7.043	6.667e − 3	0.2206	302.95	0.993	1.210	48.15
$\mathcal{J}_{14}^e$ minimax angle	17.71	0.691	2.694	6.667e − 3	0.2305	330.10	0.993	0.806	85.70
$\mathcal{J}_{15}^e$ minimax angle rate	31.31	0.189	1.616	6.667e − 3	0.2236	402.54	0.993	0.439	40.24
$\mathcal{J}_{16}^e$ Minimax angle accel.	30.93	0.341	0.221	6.667e − 3	0.4128	657.81	0.995	0.324	67.76
$\mathcal{J}_{17}^e$ minimax length rate	31.49	1.046	3.717	6.667e − 3	0.2581	701.61	0.993	0.204	70.14
$\mathcal{J}_{18}^e$ minimax unstrained length rate	31.74	1.030	3.694	6.667e − 3	0.1355	231.64	0.993	0.183	23.16
$\mathcal{J}_{19}^e$ minimax length accel.	36.51	0.446	0.651	3.058e − 3	6.439e − 2	208.52	0.997	0.269	20.85
$\mathcal{J}_{20}^e$ minimax unstrained length accel.	36.51	0.444	0.658	3.098e − 3	1.035e − 2	1.049	0.997	0.271	0.105
$\mathcal{J}_{21}^e$ minimax strain	48.10	1.089	3.546	2.954e − 3	6.205e − 2	5.959	0.997	0.540	3.069
$\mathcal{J}_{22}^e$ minimax strain rate	35.34	0.589	1.439	3.490e − 3	6.966e − 4	0.792	0.997	0.289	0.519
$\mathcal{J}_{23}^e$ minimax strain accel.	30.26	0.389	0.546	3.336e − 3	1.448e − 3	7.054e − 4	0.997	0.257	0.371

the rigid tether results. However, as has been observed in the previous results, the converse is not true. All three of the trajectories saturate the tether strain at the upper limit and require large reel accelerations.

The minimax strain trajectory naturally produces the lowest peak in the tether strain. The trajectories are very similar to the minimax tension trajectories for the rigid tether. However, the nearly bang–bang variation in the tether strain that results makes this cost unsuitable for implementation. Surprisingly, the minimax length acceleration behaves quite poorly in terms of the maximum strain acceleration (208.5) and reel acceleration (20.85). However, the tether strain does not saturate and the required reel rate is quite reasonable. Despite the discrepancies in the maximum accelerations, the trajectory for the minimax length acceleration cost is quite smooth overall. As has been observed throughout the results, the strained and unstrained cost functions produce more or less identical libration and unstrained length variations. Although the peak accelerations for the minimax unstrained length acceleration are significantly less than the minimax length acceleration trajectory, the overall variation in the tether strain is much less smooth.

In a similar manner to the rigid tether case, a good measure of the performance of the costs can be formulated by calculating the norm of the maximum states and accelerations. However, for the elastic tether case, the states of most importance are the tether strain variables. The relative magnitudes of the strain and strain rate, however, are significantly lower than the other state variables, and so it is necessary to scale the strain variables to make the comparison meaningful.

For the states and accelerations in their original scales, the best-performing cost functions are the minimax strain acceleration, minimum strain rate, minimum length acceleration, minimum strain acceleration, and minimax unstrained length acceleration. The worst-performing costs are the minimax length rate, followed by the minimax angle acceleration. If the tether strain components are weighted more heavily (by a factor of 1000), then the top two costs remain unchanged. The third-best cost for a weighted norm of the maximum states and accelerations is the minimax strain rate, followed by the minimum strain acceleration and minimum length acceleration. For a norm based purely on the strain variables, the two best cost functions are still the minimax strain acceleration and minimum strain rate. These are followed by the minimum strain acceleration, minimum strain, and minimum strain rate. Thus, we are led to a virtually identical conclusion as in the case of a rigid tether: it is desirable to employ a cost function minimizing either the length acceleration or functions of the strain (tension) rate or strain (tension) acceleration. However, for the best combination of minimum control input and smooth longitudinal dynamics, the minimax strain acceleration is the best-performing trajectory.

2. *Sensitivity Analysis*

Table 7 summarizes the percentage change in the maximum absolute values of the key state variables for three cost functions for the elastic tether system due to changes in tether length, subsatellite mass, tether stiffness, orbit altitude, tether density, mother satellite mass, initial tether length, and initial libration angle. The results show that the librational dynamics are largely unaffected by changes in the mass distribution and orbit altitude. However, changes in mass distribution alter the tether tension and therefore different control actions are required to ensure that the longitudinal vibrations are suppressed. For example, the minimax strain acceleration trajectories show that there is a sensitive dependence of the states on tether density. The longitudinal dynamics tend to be most sensitive to changes in subsatellite mass, tether density, and tether stiffness. This is true of all configurations because of the corresponding change in the tether strain. Its impact on the overall libration motion is small, however. It can be noted that the elastic trajectories tend to be more sensitive than the optimal trajectories for a rigid tether. This is due to the changes in the longitudinal dynamics, which require larger changes in the reel acceleration to adequately control and, hence, changes in the unstrained length dynamics. Such changes are the primary reason for the differences in the librational dynamics as opposed to the longitudinal oscillations of the subsatellite directly influencing the librational modes.

VI. Conclusions

A large number of cost functions were compared for the deployment/retrieval optimization of a tethered satellite system. The symmetry of the deployment and retrieval processes was proven for both inelastic and elastic tether models, thus implying that the computation of a deployment trajectory automatically gives a corresponding retrieval trajectory. Numerical results illustrate the importance of selecting a "good" cost function for optimizing the deployment/retrieval processes. For a rigid tether, minimizing the length acceleration or minimizing functions of the tension rate or tension acceleration appear to give good trajectories in terms of the maximum variations in the states and accelerations. The situation is

Table 7 Percentage change in the maximum absolute values of state variables because of parameter variations for an elastic tether

	Minimum strain acceleration						Minimax strain rate						Minimax strain acceleration					
	$\Delta\theta'_{max}$	$\Delta\theta''_{max}$	$\Delta\varepsilon'_{max}$	$\Delta\varepsilon''_{max}$	$\Delta\Lambda'_{max}$	$\Delta\Lambda''_{max}$	$\Delta\theta'_{max}$	$\Delta\theta''_{max}$	$\Delta\varepsilon'_{max}$	$\Delta\varepsilon''_{max}$	$\Delta\Lambda'_{max}$	$\Delta\Lambda''_{max}$	$\Delta\theta'_{max}$	$\Delta\theta''_{max}$	$\Delta\varepsilon'_{max}$	$\Delta\varepsilon''_{max}$	$\Delta\Lambda'_{max}$	$\Delta\Lambda''_{max}$
Tether length																		
20 km	−0.70	−1.36	−83.17	−47.05	1.22	0.95	−0.70	−2.32	−81.22	−73.14	0.82	9.34	0.55	−1.10	−80.94	−80.82	1.56	7.57
50 km	−0.40	−0.82	−54.98	−65.81	0.77	0.63	−0.33	−1.43	−51.95	−39.21	0.43	1.40	0.30	−0.72	−51.45	−51.26	0.94	4.49
150 km	0.52	0.87	64.83	45.33	−0.68	−0.31	0.04	1.13	55.74	21.72	−0.43	−7.00	−0.39	0.76	54.20	53.69	−0.88	−3.81
200 km	1.05	1.72	138.37	120.58	−1.33	−0.69	0.38	2.31	115.15	85.13	−0.85	−8.65	−0.68	1.54	110.86	109.79	−1.67	−7.07
250 km	1.67	2.59	215.82	219.48	−1.93	−1.38	0.51	3.28	178.10	104.04	−1.20	−11.73	−0.97	2.32	169.78	168.23	−2.42	−9.91
300 km	2.22	3.40	303.55	323.14	−2.53	−2.31	0.46	4.06	244.49	116.72	−1.57	−12.23	−1.28	3.12	230.99	228.90	−3.10	−12.37
Subsatellite mass																		
100 kg	7.24	8.19	−62.34	28.50	−1.10	0.61	2.02	7.48	−70.18	−48.83	−0.69	−8.34	4.30	10.67	−72.55	−72.75	−4.20	−21.31
200 kg	3.39	3.68	−46.51	−52.82	−0.15	0.68	0.44	2.02	−48.99	8.87	−0.06	−5.20	−0.87	3.75	−53.32	−53.55	−1.89	−10.55
300 kg	2.02	2.03	−30.73	−37.46	0.24	0.84	0.52	1.89	−33.83	9.57	−0.20	−4.64	−0.58	1.62	−34.79	−35.06	−0.88	−5.23
400 kg	1.43	1.30	−15.79	−25.30	0.51	0.84	0.15	0.72	−16.60	4.23	−0.06	−1.54	−0.22	0.60	−17.07	−17.21	−0.35	−2.07
600 kg	0.47	0.27	12.97	2.10	0.49	0.49	−0.15	−0.53	16.01	−12.70	0.02	0.94	0.13	−0.40	16.46	16.59	0.22	1.45
700 kg	0.35	0.12	26.69	13.44	0.55	0.51	−0.29	−0.94	31.46	−12.69	0.01	1.13	0.22	−0.67	32.34	32.60	0.37	2.52
800 kg	0.31	0.06	39.96	26.49	0.61	0.52	−0.40	−1.25	46.38	−9.82	0.01	0.94	0.28	−0.88	47.66	48.07	0.47	3.33
900 kg	0.26	−0.00	52.86	37.41	0.63	0.50	−0.49	−1.50	60.80	−0.94	0.02	0.60	0.32	−1.04	62.47	63.11	0.55	3.96
1000 kg	0.29	0.01	65.01	49.38	0.67	0.48	−0.58	−1.70	74.74	7.66	0.02	0.14	0.38	−1.16	76.78	77.45	0.60	4.46
Tether stiffness																		
20,000 N	0.28	0.73	203.56	198.01	−1.01	−0.92	−0.03	−0.07	199.77	1052.6	−0.53	1526.4	0.00	−0.07	199.84	199.96	−0.53	−0.97
30,000 N	0.13	0.40	103.32	80.44	−0.49	−0.29	−0.01	−0.00	99.97	34.70	−0.26	−4.27	−0.00	−0.04	99.97	99.96	−0.26	−0.48
40,000 N	0.07	0.21	51.71	36.71	−0.24	−0.11	−0.00	0.00	49.99	4.20	−0.13	−3.87	0.00	−0.02	49.98	49.98	−0.13	−0.24
50,000 N	0.05	0.10	20.60	14.10	−0.09	−0.03	−0.00	−0.00	19.99	4.19	−0.05	−2.13	0.00	−0.01	19.99	19.99	−0.05	−0.10
70,000 N	1.30	0.85	−17.49	−24.18	0.79	0.43	0.00	0.00	−14.28	−10.10	0.04	0.10	−0.00	0.01	−14.28	−14.29	0.04	0.07
80,000 N	2.31	1.15	−32.86	−32.20	1.23	−2.38	0.00	0.00	−25.00	−10.10	0.07	−0.31	−0.00	0.01	−24.99	−24.99	0.07	0.12
90,000 N	2.45	1.23	−40.98	−48.80	1.33	−2.53	0.00	0.01	−33.33	−10.10	0.09	−0.54	−0.00	0.01	−33.33	−33.33	0.09	0.16
100,000 N	2.68	1.28	−48.05	−57.82	1.40	−3.53	0.01	0.01	−39.99	−10.10	0.11	−0.54	−0.00	0.01	−39.99	−40.00	0.11	0.19
Altitude																		
300 km	1.23	0.93	7.30	−6.08	0.63	0.57	−0.00	−0.01	9.26	6.04	−0.03	−0.51	0.00	−0.00	9.25	9.25	−0.02	−0.04
400 km	1.08	0.84	2.91	−6.90	0.59	0.66	−0.00	−0.00	4.49	6.04	−0.01	−0.26	0.00	−0.00	4.49	4.48	−0.01	−0.02
600 km	0.90	0.70	−5.29	−17.07	0.56	0.65	0.00	0.00	−4.23	−0.00	0.01	0.15	−0.00	0.00	−4.23	−4.25	0.01	0.02
700 km	2.02	1.26	−14.88	−21.82	1.10	−0.68	0.00	0.01	−8.23	−0.00	0.02	0.15	−0.00	0.00	−8.24	−8.25	0.02	0.04
800 km	2.85	1.62	−21.62	−32.11	1.45	−2.54	0.00	0.01	−12.01	−0.00	0.04	0.15	−0.00	0.00	−12.02	−12.03	0.03	0.06
900 km	3.69	2.13	−28.36	−37.37	1.87	−4.54	0.01	0.02	−15.58	−0.00	0.05	0.15	−0.00	0.01	−15.60	−15.60	0.04	0.08
1000 km	4.77	2.62	−35.65	−47.69	2.36	−7.20	0.01	0.02	−18.96	−0.01	0.06	0.05	−0.00	0.01	−18.98	−18.99	0.05	0.09
Tether density																		
2 kg/km	1.27	1.58	16.39	4.61	−0.58	−0.10	0.39	2.36	7.53	192.29	−0.61	−6.10	−0.68	1.59	5.46	4.93	−1.40	−6.61
3 kg/km	2.21	2.81	32.16	23.15	−1.16	−0.27	0.41	3.83	14.79	190.42	−1.07	−7.49	−1.29	3.25	10.42	9.73	−2.58	−11.47
4 kg/km	3.11	3.93	46.92	44.61	−1.58	−0.36	0.38	4.72	21.77	188.62	−1.53	−10.86	0.04	5.04	15.20	14.37	−3.54	−15.14
5 kg/km	3.88	4.89	61.27	64.80	−1.92	−0.41	0.18	5.14	28.46	186.89	−1.92	−11.67	1.30	6.71	19.81	18.88	−4.41	−17.95
6 kg/km	4.57	5.74	74.72	81.29	−2.18	−0.47	−0.05	5.97	34.82	278.28	−2.25	−11.63	2.48	8.28	24.25	23.22	−5.13	−20.14
7 kg/km	5.35	6.57	87.32	85.78	−2.33	−0.85	−0.28	6.33	40.98	295.52	−2.61	−10.30	3.57	9.71	28.51	27.41	−5.79	−21.84
8 kg/km	5.89	7.21	98.95	99.02	−2.47	−0.87	−0.27	6.50	46.86	293.96	−2.90	−8.87	4.55	11.01	32.59	31.40	−6.39	−23.17
9 kg/km	6.37	7.77	110.08	110.28	−2.54	−0.89	−0.32	6.51	52.49	292.45	−3.18	−7.75	5.43	12.18	36.48	35.23	−6.95	−24.20
10 kg/km	6.80	8.27	120.37	118.50	−2.57	−0.91	−0.39	6.44	57.82	291.00	−3.46	−6.93	6.21	13.22	40.22	38.87	−7.45	−24.97

(continued)

Table 7 Percentage change in the maximum absolute values of state variables because of parameter variations for an elastic tether (Continued)

	Minimum strain acceleration						Minimax strain rate						Minimax strain acceleration					
	$\Delta\theta'_{max}$	$\Delta\theta''_{max}$	$\Delta\varepsilon'_{max}$	$\Delta\varepsilon''_{max}$	$\Delta\Lambda'_{max}$	$\Delta\Lambda''_{max}$	$\Delta\theta'_{max}$	$\Delta\theta''_{max}$	$\Delta\varepsilon'_{max}$	$\Delta\varepsilon''_{max}$	$\Delta\Lambda'_{max}$	$\Delta\Lambda''_{max}$	$\Delta\theta'_{max}$	$\Delta\theta''_{max}$	$\Delta\varepsilon'_{max}$	$\Delta\varepsilon''_{max}$	$\Delta\Lambda'_{max}$	$\Delta\Lambda''_{max}$
Mother satellite mass																		
2500 kg	0.32	−0.06	−14.39	−23.56	0.65	0.12	−0.40	−0.39	−9.69	−0.00	−0.07	0.33	0.14	−0.83	−9.60	−9.61	0.03	1.27
7500 kg	0.74	0.66	3.52	−9.25	0.28	0.45	0.15	0.15	3.64	0.00	0.03	−0.55	−0.04	0.27	3.60	3.62	−0.01	−0.42
10,000 kg	2.28	1.71	2.06	−7.75	0.99	0.15	0.23	0.22	5.54	9.98	0.04	−0.75	−0.05	0.40	5.49	5.50	−0.02	−0.62
25,000 kg	2.79	1.88	1.59	2.17	0.99	−1.24	0.38	0.36	9.13	9.98	0.06	−1.29	−0.09	0.64	9.05	9.13	−0.03	−1.01
50,000 kg	3.53	2.41	1.90	−2.78	1.34	−1.62	0.43	0.40	10.37	20.91	0.07	−1.59	−0.09	0.72	10.28	10.29	−0.04	−1.12
Initial length																		
5 km	21.23	18.25	−32.20	291.19	12.94	16.53	36.33	36.13	−27.06	104.75	12.74	21.30	43.09	66.67	−33.79	−31.09	1.45	14.59
6 km	15.22	12.91	−34.68	195.30	9.38	11.98	27.04	25.22	−31.41	92.56	9.21	13.12	31.54	47.68	−35.63	−33.41	1.65	10.88
7 km	10.46	8.74	−37.05	98.59	6.52	8.13	18.42	16.93	−34.56	51.54	6.32	6.94	21.27	32.49	−36.63	−35.40	1.53	7.69
8 km	6.42	5.30	−38.61	64.12	4.11	5.06	11.54	10.31	−36.89	28.97	3.86	4.09	12.00	19.86	−38.05	−37.11	1.21	4.91
9 km	3.02	2.42	−39.59	6.67	2.07	2.38	5.41	4.74	−38.64	−24.47	1.85	1.75	3.77	9.14	−39.20	−38.62	0.72	2.45
Initial angle																		
−20 deg	−10.71	45.70	−44.17	36.17	−6.53	−6.12	−9.95	−20.31	−44.04	−0.01	−4.31	−8.44	−24.14	76.69	−45.84	−45.82	−3.48	−19.22
−15 deg	−8.45	10.71	−43.50	20.73	−5.08	−4.72	−8.11	−15.15	−43.07	−0.01	−3.30	−6.57	−15.19	43.69	−43.74	−44.00	−2.70	−11.85
−10 deg	−5.98	−5.21	−42.59	4.36	−3.52	−3.09	−5.80	−10.00	−42.06	−0.01	−2.21	−5.58	−5.81	26.97	−42.14	−42.59	−1.28	−4.07
−5 deg	−3.16	−2.83	−41.60	−28.10	−1.75	−1.50	−3.04	−5.11	−41.03	−0.01	−1.07	−3.49	−2.86	14.11	−40.94	−41.27	−0.55	−1.89
5 deg	3.93	3.16	−38.43	45.78	2.59	3.36	8.29	5.09	−38.97	7.63	1.28	0.32	8.96	−12.81	−39.28	−38.84	0.70	2.10
10 deg	8.43	6.98	−35.96	117.37	5.29	7.07	18.94	10.12	−37.93	7.63	2.46	1.80	24.32	−1.68	−38.65	−37.89	1.25	3.74
15 deg	13.79	23.34	−33.60	167.15	8.47	11.32	30.16	15.02	−36.87	7.63	3.66	3.45	44.41	37.44	−37.94	−37.07	1.77	5.16
20 deg	20.36	60.27	−31.26	269.65	12.26	16.64	41.88	20.17	−35.72	80.58	4.93	5.35	68.04	76.69	−36.80	−35.78	2.10	7.31

even more critical for an elastic tether, for which the longitudinal dynamics of the tether can be critical. It is necessary to incorporate functions of the tether strain rate and strain acceleration into the cost function. In particular, minimax strain acceleration proves to be the best cost function when compared in terms of the maximum states and accelerations. For both rigid and elastic tethers, minimizing the length acceleration was found to be a very good measure of the system performance as well. Hence, optimal deployment/retrieval trajectories are categorized by similar cost functions for both rigid and elastic tethers. The results show that the elastic tether behaves in a similar manner to the rigid only if an appropriate cost function is selected for the elastic tether. For the best-performing cost functions, changes in the system mass distribution have only minor effects on the reel dynamics. Changes in the initial angle of the tether alter the peak dynamics, but do not significantly change the nature of the optimal trajectories. These results should form the basis for the selection of cost functions for future tethered satellite missions.

Acknowledgments

Portions of this work were originally carried out under the supervision of Pavel Trivailo at RMIT University. The author would like to thank the reviewers for their valuable comments.

References

[1] Cosmo, M. L., and Lorenzini, E. C., *Tethers in Space Handbook*, 3rd ed., Smithsonian Astrophysical Observatory, Cambridge, MA, Dec. 1997.

[2] Nordley, G. D., and Forward, R. L., "Mars–Earth Rapid Interplanetary Tether Transport System I—Initial Feasibility Analysis," *Journal of Propulsion and Power*, Vol. 17, No. 3, 2001, pp. 499–507.

[3] Lorenzini, E. C., Cosmo, M. L., Kaiser, M., Bangham, M. E., Vonderwell, D. J., and Johnson, L., "Mission Analysis of Spinning Systems for Transfers from Low Orbits to Geostationary," *Journal of Spacecraft and Rockets*, Vol. 37, No. 2, 2000, pp. 165–172.

[4] Williams, P., Blanksby, C., and Trivailo, P., "Tethered Planetary Capture Maneuvers," *Journal of Spacecraft and Rockets*, Vol. 41, No. 4, 2004, pp. 603–613.

[5] Johnson, L., Estes, R. D., Lorenzini, E. C., Martinez-Sanchez, M., Sanmartin, J., and Vas, I., "Electrodynamic Tethers for Spacecraft Propulsion," AIAA Paper 98-0983, Aug. 1998.

[6] Tragesser, S. G., and San, H., "Orbital Maneuvering with Electrodynamic Tethers," *Journal of Guidance, Control, and Dynamics*, Vol. 26, No. 5, 2003, pp. 805–810.

[7] Pearson, J., Levin, E., Carroll, J. A., and Oldson, J. C., "Orbital Maneuvering with Spinning Electrodynamic Tethers," AIAA Paper 2004-5715, Aug. 2004.

[8] Williams, P., "Optimal Orbit Transfer with Electrodynamic Tether," *Journal of Guidance, Control, and Dynamics*, Vol. 28, No. 2, 2005, pp. 369–372.

[9] Misra, A. K., and Modi, V. J., "A Survey of the Dynamics and Control of Tethered Satellite Systems," *Advances in the Astronautical Sciences*, Vol. 62, Univelt, Inc., San Diego, CA, 1987, pp. 667–719.

[10] Williams, P., "Nonlinear Control and Applications of Tethered Space Systems," Ph.D. Dissertation, School of Aerospace, Mechanical, and Manufacturing Engineering, Royal Melbourne Institute of Technology, Melbourne, Australia, 2004.

[11] Williams, P., Blanksby, C., Trivailo, P., and Fujii, H. A., "Receding Horizon Control of Tether System Using Quasilinearisation and Chebyshev Pseudospectral Approximations," *Advances in the Astronautical Sciences*, Vol. 116, Pt. 1, 2003, pp. 539–558.

[12] Williams, P., Blanksby, C., and Trivailo, P., "Optimisation of Tether Assisted Sample Return from the International Space Station," Australian International Aerospace Congress Paper 2003-021, July–Aug. 2003.

[13] Misra, A. K., and Modi, V. J., "Deployment and Retrieval of Shuttle Supported Tethered Satellites," *Journal of Guidance, Control, and Dynamics*, Vol. 5, No. 3, 1982, pp. 278–285.

[14] Fujii, H., and Ishijima, S., "Mission Function Control for Deployment and Retrieval of a Subsatellite," *Journal of Guidance, Control, and Dynamics*, Vol. 12, No. 2, 1989, pp. 243–247.

[15] Fujii, H., Uchiyama, K., and Kokubun, K., "Mission Function Control of Tethered Subsatellite Deployment/Retrieval: In-Plane and Out-of-Plane Motion," *Journal of Guidance, Control, and Dynamics*, Vol. 14, No. 2, 1991, pp. 471–473.

[16] Vadali, S. R., and Kim, E. S., "Feedback Control of Tethered Satellites Using Lyapunov Stability Theory," *Journal of Guidance, Control, and Dynamics*, Vol. 14, No. 4, 1991, pp. 729–735.

[17] Fujii, H. A., and Anazawa, S., "Deployment/Retrieval Control of Tethered Subsatellite Through an Optimal Path," *Journal of Guidance, Control, and Dynamics*, Vol. 17, No. 6, 1994, pp. 1292–1298.

[18] Bainum, P. M., and Kumar, V. K., "Optimal Control of the Shuttle-Tethered-Subsatellite System," *Acta Astronautica*, Vol. 7, Nov.–Dec. 1980, pp. 1333–1348. doi:10.1016/0094-5765(80)90010-7

[19] Steindl, A., and Troger, H., "Optimal Control of Deployment of a Tethered Subsatellite," *Nonlinear Dynamics*, Vol. 31, No. 3, 2003, pp. 257–274. doi:10.1023/A:1022956002484

[20] Williams, P., Blanksby, C., and Trivailo, P., "Optimal Control of Flexible Tethers," International Astronautical Congress Paper 03-A.6.05, Sept.–Oct. 2003.

[21] Lakso, J. J., and Coverstone, V. L., "Optimal Tether Deployment/Retrieval Trajectories Using Direct Collocation," AIAA Paper 2000-4349, Aug. 2000.

[22] Barkow, B., Steindl, A., Troger, H., and Wiedermann, G., "Various Methods of Controlling the Deployment of a Tethered Satellite," *Journal of Vibration and Control*, Vol. 9, Nos. 1–2, 2003, pp. 187–208. doi:10.1177/1077546303009001747

[23] Koakutsu, H., Nakajima, A., Ota, S., and Nakasuka, S., "Tension Control of Micro Tether System on Circular Orbit Considering Tether Flexibility," *Journal of Space Technology and Science*, Vol. 12, No. 2, 1996, pp. 1–13.

[24] Zimmerman, F., Schottle, U. M., and Messerschmid, E., "Optimal Deployment and Return Trajectories for a Tether-Assisted Re-Entry Mission," AIAA Paper 99-4168, Aug. 1999.

[25] Andres, Y. N., Zimmerman, F., and Schottle, U. M., "Optimization and Control of the Early Deployment Phase During a Tether Assisted Deorbit Maneuver," *Proceedings of the 22nd International Symposium on Space Technology and Science, Japan Society for Aeronautical and Space Sciences and 22nd ISTS Organizing Committee*, 2002, pp. 1795–1800;also ISTS Paper 2000-k-22v.

[26] Nagata, T., "Simultaneous Optimization of the Orbit and the Subsatellite Swing for a Tethered System," American Astronautical Society Paper 97-484, July 1997.

[27] Fujii, H. A., and Kojima, H., "Optimal Trajectory Analysis for Deployment/Retrieval of Tethered Subsatellite Using Metric," *Journal of Guidance, Control, and Dynamics*, Vol. 26, No. 1, 2003, pp. 177–179.

[28] Stuart, D. G., "Guidance and Control for Cooperative Tether-Mediated Orbital Rendezvous," *Journal of Guidance, Control, and Dynamics*, Vol. 13, No. 6, 1990, pp. 1102–1108.

[29] Ross, I. M., "How to Find Minimum-Fuel Controllers," AIAA Paper 2004-5346, Aug. 2004.

[30] Bryson, A. E., and Ho, Y. C., *Applied Optimal Control*, Hemisphere, New York, 1975.

[31] Betts, J. T., *Practical Methods for Optimal Control Using Nonlinear Programming*, Advances in Control and Design Series, Society for Industrial and Applied Mathematics, Philadelphia, 2001.

[32] Hargraves, C. R., and Paris, S. W., "Direct Trajectory Optimization Using Nonlinear Programming and Collocation," *Journal of Guidance, Control, and Dynamics*, Vol. 10, No. 4, 1987, pp. 338–342.

[33] Elnagar, G., Kazemi, M. A., and Razzaghi, M., "The Legendre Pseudospectral Method for Discretizing Optimal Control Problems," *IEEE Transactions on Automatic Control*, Vol. 40, No. 10, 1995, pp. 1793–1796. doi:10.1109/9.467672

[34] Ross, M., and Fahroo, F., Legendre Pseudospectral Approximations of Optimal Control Problems, *New Trends in Nonlinear Dynamics and Control, and Their Applications*, edited by W. Kang, M. Xiao, and C. Borges, Vol. 295, Lecture Notes in Control and Information Sciences, Springer–Verlag, Berlin/Heidelberg, 2003, pp. 327–342.

[35] "User's Guide to DIRECT Version 1.18," Rept. TR-0301.01, RMIT University, School of Aerospace, Mechanical, and Manufacturing, Melbourne, Australia, Jan. 2006.

[36] Gill, P. E., Murray, W., and Saunders, M. A., "SNOPT: An SQP Algorithm for Large-Scale Constrained Optimization," *SIAM Journal on Optimization*, Vol. 12, No. 4, 2002, pp. 979–1006. doi:10.1137/S1052623499350013

C. McLaughlin
Associate Editor